



Deposited via The University of Sheffield.

White Rose Research Online URL for this paper:

<https://eprints.whiterose.ac.uk/id/eprint/232271/>

Version: Accepted Version

Article:

Rahman, M.M., Watton, P.N., Neu, C.P. et al. (2025) Predicting the heterogeneous chemo-mechano-biological degeneration of cartilage using 3-D biphasic finite elements. *Computer Methods and Programs in Biomedicine*, 270. 108902. ISSN: 0169-2607

<https://doi.org/10.1016/j.cmpb.2025.108902>

© 2025 The Authors. Except as otherwise noted, this author-accepted version of a journal article published in *Computer Methods and Programs in Biomedicine* is made available via the University of Sheffield Research Publications and Copyright Policy under the terms of the Creative Commons Attribution 4.0 International License (CC-BY 4.0), which permits unrestricted use, distribution and reproduction in any medium, provided the original work is properly cited. To view a copy of this licence, visit <http://creativecommons.org/licenses/by/4.0/>

Reuse

This article is distributed under the terms of the Creative Commons Attribution (CC BY) licence. This licence allows you to distribute, remix, tweak, and build upon the work, even commercially, as long as you credit the authors for the original work. More information and the full terms of the licence here: <https://creativecommons.org/licenses/>

Takedown

If you consider content in White Rose Research Online to be in breach of UK law, please notify us by emailing eprints@whiterose.ac.uk including the URL of the record and the reason for the withdrawal request.

Predicting the heterogeneous chemo-mechano-biological degeneration of cartilage using 3-D biphasic finite elements

Muhammed Masudur Rahman^a, Paul N. Watton^{b,c}, Corey P. Neu^{d,e,f}, David M. Pierce^{a,g,*}

^aDepartment of Mechanical Engineering, University of Connecticut, Storrs, CT, USA

^bDepartment of Computer Science & Insigneo Institute for in silico Medicine, University of Sheffield, Sheffield, UK

^cDepartment of Mechanical Engineering and Materials Science, University of Pittsburgh, Pittsburgh, US

^dPaul M. Rady Department of Mechanical Engineering, University of Colorado, Boulder, CO, USA

^eBiomedical Engineering Program, University of Colorado, Boulder, CO, USA

^fBioFrontiers Institute, University of Colorado, Boulder, CO, USA

^gDepartment of Biomedical Engineering, University of Connecticut, Storrs, CT, USA

Abstract

Background and Objective: Osteoarthritis (OA), a debilitating joint disease, involves progressive cartilage degeneration and altered biomechanics. We established a novel chemo-mechano-biological (CMB) modeling framework that integrates biphasic mechanics with biochemical and biological processes to predict cartilage degeneration (i.e. loss of masses of constituents presenting as loss of thickness) under pathological conditions. Our framework captures time-dependent remodeling of cartilage constituents in 3-D driven by mechanical loading, biochemical signaling, and cellular metabolism.

Methods: We formulated a nonlinear, large-strain biphasic constitutive model coupled with a biochemical model of signaling pathways. Our framework incorporates depth-dependent metabolic activity, explicitly linking oxygen availability to chondrocyte behavior and extracellular matrix (ECM) remodeling. We included interactions among mechanical stimuli, growth factors, pro-inflammatory cytokines, enzymes (collagenases and aggrecanases), and inhibitors (TIMP). We conducted nonlinear, biphasic finite element (FE) simulations in 3-D, allowing for realistic representations of intra-cartilage heterogeneity. We simulated cyclic, confined compression of full-thickness cartilage, a scenario mimicking conditions *in vivo* during walking or running.

Results: Our simulations spanning 24 months presented realistic patterns of cartilage

*Corresponding author

Email address: dmpierce@engr.uconn.edu (David M. Pierce)

degeneration including zonal variations in matrix composition and thickness loss. In healthy cartilage, interstitial fluid pressure resisted mechanical loading, maintaining ECM integrity. However, in degenerative overloading conditions, enzymatic activity and altered metabolic functions led to increased porosity, reduced fluid pressure, and heterogeneous degradation of ECM. Incorporating depth-dependent metabolic activity revealed pronounced degeneration in the superficial zone (SZ) and progressively reduced loss toward the deep zone (DZ). This outcome aligns with experimental evidence on progression of OA. Oxygen availability played a critical role, with higher levels exacerbating degradation, consistent with findings linking oxidative stress to cartilage degeneration.

Conclusions: Our nonlinear, biphasic FE framework offers a robust tool for investigating mechanisms of cartilage degeneration and OA, and advancing therapeutic strategies. It uniquely integrates biphasic mechanics, signaling pathways, and metabolic activity in 3-D, providing insights into patterns of cartilage degeneration. We previously developed automated and publicly available tools to generate patient-specific knee models from MR Images, altogether enabling personalized diagnostics/prognostics and pre-/post-operative planning. Our CMB framework is also publicly available as a plugin for FEBio at <https://github.uconn.edu/imLab/FEVGnR-Plugin>, supporting broader research on OA and cartilage biomechanics.

Keywords: cartilage, mechanobiology, mathematical modeling, growth and remodeling, osteoarthritis, metabolism

1. Introduction

Degeneration of articular cartilage caused by, e.g. injuries, repetitive stresses, age-related changes, and joint misalignments, ultimately results in loss of function and likely contributes to development of osteoarthritis (OA). OA is a chronic whole-joint disease affecting millions
5 of people worldwide, where degeneration of cartilage plays a prominent role [1]. Progressive degeneration, causing loss of cartilage and cartilage function, leads to failure of the synovial joint, affecting quality of life through pain, functional limitations, lost earnings, anxiety, and depression [2]. Despite the prevalence and impact of OA, and an enormous body of literature on cartilage mechanics and OA, we understand neither the cause nor progression

10 of the disease and treatment remains primarily symptomatic. No cure yet exists.

Articular cartilage, a multiphase soft tissue, comprises by percentage wet weight, fluid and electrolytes (68-85%), collagen fibers (15-25%), proteoglycans (5-10%), and chondrocytes (primary cell type, <4%) [3]. The heterogeneous solid phase of cartilage is an extracellular matrix (ECM), consisting of a mesh of negatively charged proteoglycan entangled in a
15 network of primarily type II collagen fibers. The remarkable mechanics of cartilage derive from the complex interactions of proteoglycans, collagens, and electrolytic fluid. In particular these interactions facilitate fluid retention within the ECM, generating interstitial fluid pressure crucial to shield the solid matrix from mechanical load and to facilitate low-friction articulation [4, 5].

20 Intra-tissue biomechanics also play a vital role in the development, homeostasis, pathology, and regeneration of articular cartilage. Chondrocytes maintain a homeostatic balance between the degradation and synthesis of ECM under normal physiological mechanical stimuli [6]. Such mechanical stimuli are generally cyclic (mixed compression, tension, and hydrostatic pressure) and increase synthesis of both collagen and proteoglycan
25 [7–11]. However, excessive mechanical loading is detrimental to cartilage, causing softening, fibrillation, ulceration, and erosion [6, 9, 12, 13]. Interestingly, lack of mechanical stimuli, e.g. long-term immobilization, reduces synthesis of structural proteins and increases pro-inflammatory cytokines, altogether presenting as thinning of cartilage [9, 14–16]. Both amplitude and frequency of loading affect the production/degradation of cartilage
30 constituents [10, 17, 18].

Chondrocytes, relatively inert in healthy conditions, “activate” under pathological conditions and alter their functional behavior, which changes the homeostatic balance between synthesis and degradation of ECM constituents [1, 13, 19]. Chondrocytes, and other cells within the synovial joint, produce pro-inflammatory cytokines, e.g. interleukin
35 IL-1 β , IL-6, IL-18, tumor necrosis factor TNF- α , that upregulate collagenases (matrix metalloproteinases, MMPs) and aggrecanases (a disintegrin and metalloproteinase with thrombospondin motifs, ADAMTSs) [1, 13, 19, 20]. These proteases degrade collagen and proteoglycan, which alters fluid-pressure retention and load-bearing function of cartilage, thus affecting mechanotransduction and mechanobiology [16]. Moreover, pro-inflammatory

40 cytokines cause apoptosis and necrosis of chondrocytes [21], another hallmark feature of OA
[9, 22, 22–27]. In response chondrocytes express growth factors (e.g. transforming growth
factors, TGF- β 1, 2, 3; activins; bone morphogenetic protein, BMPs; growth/differentiation
factors, GDFs) and tissue inhibitors of metalloproteinases (TIMPs), which oppose the
catabolic activities of pro-inflammatory cytokines and proteases [28, 29]. Nevertheless, this
45 attempt at counter-balancing is generally insufficient to revert to normal health.

Compounding such efforts, chondrocytes generally reside in a hypoxic environment, i.e.
where the level of oxygen level is relatively low [30]. The oxygen concentration in cartilage is
higher in the superficial zone (SZ) at \sim 10% compared to deep zone (DZ) at \sim 1%, as cartilage
apparently receives nutrients and oxygen mostly from synovial fluid [13]. Experimental
50 evidence on chondrocyte metabolism suggests that hypoxia (\sim 5%) reduces production of
collagenases, and corresponding degradation of type II collagen, while normoxic condition
(\sim 20%) increases both production of collagen and collagenases [31]. Thus, in the presence
of nutrients, oxygen facilitates the metabolism of chondrocytes [32]. Both anabolic and
catabolic activities of chondrocytes in OA depend on the availability of oxygen, and both
55 maintenance of homeostasis and progression of disease evolve heterogeneously through the
thickness of cartilage [33].

Models of cartilage in health and in OA provide a means to synthesize diverse
experimental data and provide new insights to structure-function relationships, disease
progression, and even treatment targets. Previous computational growth and remodeling
60 models captured changes in the volume and composition of both natural and engineered
cartilage, including mechanical damage, but neglected chemical factors [34–40]. Conversely,
models focused on the biochemical pathways of cartilage neglected mechanical stimulation
[41, 42]. Some recent models of cartilage combined effects of mechanical and chemo-biological
stimuli to simulate degeneration of cartilage over days, facilitating comparisons with
65 experimental data *ex vivo* [43–45]. We recently established a computational framework fully
coupling “minimally essential” chemo-mechano-biological effects to predict the long-term
(years) evolution of cartilage in health, disease, injury, and treatment, and provided
simplified examples [46]. However, no modeling frameworks for cartilage currently
couple mechanical, chemical, and biological perspectives to simulate the heterogeneous,

70 multi-factorial pathogenesis and long-term progression of OA in three-dimensions (3-D) despite extensive, related experimental research [47].

In this study, we establish a computational framework for modeling the coupled evolution of chemical, mechanical, and biological constituents of cartilage resulting from intra-tissue mechanical and chemical stimuli resulting in heterogeneous, volumetric changes, as well
75 as changes in organization of constituents. Here we establish our previously published biochemical pathways model [46] within 3-D biphasic finite elements by leveraging our image-driven constitutive model of cartilage [48, 49]. We also incorporate both homeostatic adaptation of cells (cells adapt to pathological or non-physiological stimuli) and novel, depth-dependent metabolic activity (metabolic activity of cells depends on the local
80 oxygen concentration). We exercise our extended computational framework to predict the heterogeneous, chemo-mechano-biological evolution of constituents in cartilage, and the resulting volumetric loss, under pathological overloading conditions. Finally, using three numerical studies we compare our predictions of degeneration (i.e. loss of masses of collagen and proteoglycan presenting as loss of thickness) over 24 months with histological assessments
85 of cartilage during the progression of early-stage OA [26]. Our CMB framework is publicly available as a plugin for FEBio at <https://github.uconn.edu/imLab/FEVGnR-Plugin>, supporting broader research on OA and cartilage biomechanics.

2. Methods

Here we extend our chemo-mechano-biological framework for modeling the evolution of
90 cartilage [46] by implementing it within 3-D biphasic finite elements and coupling it with our well-established, image-driven constitutive model of cartilage [48, 49], as this provides better insights into intra-tissue cartilage mechanics and their relation with the evolution of structural and biochemical constituents. For a conceptual overview of the modeling framework, see Fig. 1 in [46]. Here we also incorporate both homeostatic adaptation of
95 cells (as presented previously [46]) and metabolic activity of cells dependent on intra-tissue oxygen concentration (a new source of through-thickness heterogeneity).

2.1. Model formulation I: Biomechanical model of cartilage

2.1.1. Anisotropic description of growth

We utilize the very different time scales between daily activities, e.g. walking (t in
 100 seconds), and progression of damage and OA in cartilage (τ occurring over months or
 years). Accordingly, we perform a multiplicative decomposition of the total deformation
 gradient using these two time scales $\mathbf{F}(\tau, t) = \mathbf{F}_S(t)\mathbf{F}^g(\tau)$ and following our prior work
 [46], cf. Fig. 2 therein. In response to external, mechanical loading cartilage deforms
 poro-visco-elastically with $\mathbf{F}_S = \partial\mathbf{x}_S/\partial\mathbf{X}_S$ the deformation gradient tensor of the solid
 105 (subscript S), where \mathbf{x} is the position vector of the spatial point (reference position \mathbf{X}). In
 response to biomechanical and biochemical stimuli within cartilage chondrocytes excrete and
 degrade structural and biochemical constituents resulting in changes to the organization and
 volume. The (volumetric) growth deformation gradient $\mathbf{F}^g(\tau)$ captures volumetric changes
 $\det \mathbf{F}^g = \hat{v}(\tau)$, where \hat{v} is the normalized volume change. To model the degradation of
 110 cartilage, we formulate through-thickness volume growth (TVG) as [50]

$$\mathbf{F}^g = \mathbf{I} + (\hat{v} - 1)\mathbf{n} \otimes \mathbf{n}, \quad (1)$$

where \mathbf{I} is the second-order identity tensor and \mathbf{n} represents a distribution of unit vectors
 normal to the subchondral bone at the interface to cartilage.

2.1.2. Biomechanical constitutive model

We utilize the theory of porous media to model cartilage as a biphasic (poro-visco-elastic)
 115 continuum $\phi = \phi^S + \phi^F$ consisting of a porous solid phase ϕ^S saturated with the
 interstitial fluid phase ϕ^F , both materially incompressible [51, 52]. We thus characterize
 the microstructure of cartilage with the average volume fractions $n^\alpha(\mathbf{x}, t) = dv^\alpha/dv$,
 $\sum_\alpha n^\alpha(\mathbf{x}, t) = 1$, $\alpha \in S, F$, where t is time, dv^α are volume elements of the phases, dv
 is the bulk volume element, and S and F denote the solid and fluid phases, respectively. We
 120 express the total Cauchy stress as [48, 49]

$$\boldsymbol{\sigma} = -p\mathbf{I} + \boldsymbol{\sigma}_E^S = -p\mathbf{I} + 2\rho^S \mathbf{F}_S \frac{\partial \Psi^S}{\partial \mathbf{C}_S} \mathbf{F}_S^T, \quad (2)$$

where p is the fluid pore pressure, $\boldsymbol{\sigma}_E^S$ is the effective Cauchy stress tensor, ρ^S is the current
 partial density of the solid, $\mathbf{C}_S = \mathbf{F}_S^T \mathbf{F}_S$ is the right Cauchy–Green tensor, and Ψ^S is the
 solid Helmholtz free-energy function.

We employ an additive decomposition of the superimposed solid Helmholtz free-energy function Ψ^S consisting of a Donnan osmotic part Ψ_{OP}^S , and isotropic ground matrix part Ψ_{IM}^S , and a fiber network part Ψ_{FN}^S as

$$\Psi^S = \Psi_{\text{OP}}^S(J_S) + (1 - \nu(\tau))\hat{\rho}_{\text{pg}}\Psi_{\text{IM}}^S(J_S, I_1) + \nu(\tau)\hat{\rho}_{\text{co}}\Psi_{\text{FN}}^S(\mathbf{C}_S), \quad (3)$$

where $J_S = \det \mathbf{F}_S$ is the solid Jacobian, $I_1 = \text{tr} \mathbf{C}_S$ is the first invariant of \mathbf{C}_S , $\nu(\tau) = (\nu^0 \hat{m}_{\text{co}}^{\text{fn}}) / [\nu^0 \hat{m}_{\text{co}} + (1 - \nu^0) \hat{m}_{\text{pg}}]$ represents the evolving volume fraction of functional collagen with ν^0 the initial volume fraction of total collagen, and $\hat{m}_{\text{pg}}(\tau)$ and $\hat{m}_{\text{co}}(\tau) = \hat{m}_{\text{co}}^{\text{fn}}(\tau) + \hat{m}_{\text{co}}^{\text{dm}}(\tau)$ are the evolving normalized masses of proteoglycan and total collagen (with $\hat{m}_{\text{co}}^{\text{fn}}$ and $\hat{m}_{\text{co}}^{\text{dm}}$ the functional and damaged collagen, respectively, see §2.2), and $\hat{\rho}_{\text{pg}}$ and $\hat{\rho}_{\text{co}}$ are the normalized densities of proteoglycan and collagen, both respectively.

We define the evolving normalized volume change as [50]

$$\hat{v}(\tau) = \nu^0 \hat{m}_{\text{co}} + (1 - \nu^0) \hat{m}_{\text{pg}}, \quad (4)$$

where $\hat{v}(\tau = 0) = 1$. Since we model volume changes using TVG, cf. (1), \hat{v} equals the normalized change in thickness \hat{h} , see §4.

We model the strain energy of osmotic swelling as [49, 53]

$$\Psi_{\text{OP}}^S = R\Theta c_{\text{OS}}^{\text{fc}} n_{\text{OS}}^{\text{F}} \left[\frac{2\bar{c}_{\text{m}}}{c_{\text{m}}^{\text{fc}}} - \frac{\sqrt{4(\bar{c}_{\text{m}})^2 + (c_{\text{m}}^{\text{fc}})^2}}{c_{\text{m}}^{\text{fc}}} + \text{asinh} \left(\frac{c_{\text{m}}^{\text{fc}}}{2\bar{c}_{\text{m}}} \right) \right], \quad (5)$$

where, $R = 8.314 \text{ MPa} \cdot \text{mm}^3 \text{K}^{-1} \text{mol}^{-1}$ is the universal gas constant, Θ is the absolute temperature in K, and \bar{c}_{m} is the average ion concentration of the external solution. We model the concentration of the fixed charges as [49]

$$\begin{aligned} c_{\text{m}}^{\text{fc}} &= c_{\text{OS}}^{\text{fc}} n_{\text{OS}}^{\text{F}} \left(\det \mathbf{F}_S - n_{\text{OS}}^{\text{S}} \right)^{-1} \\ &= c_{\text{OS}}^{\text{fc}} \left(1 - n_{\text{OS}}^{\text{S}} \right) \left(\det \mathbf{F}_S - n_{\text{OS}}^{\text{S}} \right)^{-1}, \end{aligned} \quad (6)$$

where $c_{\text{OS}}^{\text{fc}}$ and n_{OS}^{α} are the initial concentration of fixed charges within the tissue and initial volume fractions, respectively.

We model the strain energy of the isotropic (largely) proteoglycan solid matrix [54], extended to include compaction effects, as [48, 55–57]

$$\Psi_{\text{IM}}^S(J_S, I_1) = \frac{1}{\rho_{\text{OS}}^{\text{S}}} \left[U(J_S) + \frac{1}{2} \mu^{\text{S}} (I_1 - 3) \right], \quad (7)$$

where

$$U(J_S) = \chi_{\text{cp}}^S \left[\frac{1}{2} (\log J_S)^2 + \zeta^S \right] - \mu^S \log J_S, \quad (8)$$

145 and where we use abbreviations

$$\begin{aligned} \chi_{\text{cp}}^S &= \lambda^S \left[1 + J_{\text{cp}}^S \left(1 + \frac{(J_{\text{cp}}^S)^2}{1 - J_{\text{cp}}^S} \right) \right]^{-1}, \\ \zeta^S &= J_{\text{cp}}^S \log J_S + \frac{1 - J_{\text{cp}}^S}{J_{\text{cp}}^S - 2} \\ &\quad \left[\log \frac{J_{\text{cp}}^S - J_S}{J_S (J_{\text{cp}}^S - 1) - J_{\text{cp}}^S} - \log (1 - J_{\text{cp}}^S) \right], \end{aligned} \quad (9)$$

and where μ^S is Lamé's second parameter (a stress-like material parameter corresponding to the shear modulus of the underlying matrix in the reference configuration), λ^S is Lamé's first parameter (a stress-like material parameter that degenerates to a non-physical, positive penalty parameter used to enforce incompressibility, cf. [52]), and $n_{\text{OS}}^S \leq J_{\text{cp}}^S \leq 1$ defines the
150 point of compaction for the tissue.

We model the strain energy of the networked collagen fibers as [48]

$$\Psi_{\text{FN}}^S(\mathbf{C}_S, \mathbf{M}) = \int_{\Omega} \rho(\mathbf{M}) \frac{k_1}{2k_2} \{ \exp[k_2(I_4 - 1)^2] - 1 \} \mathcal{H}(I_4 - 1) \, d\Omega, \quad (10)$$

where $\rho(\mathbf{M})$ is the angular density of fibers (the orientation distribution function) with $1/(4\pi) \int_{\Omega} \rho(\mathbf{M}) \, d\Omega = 1$ (where $\Omega = \mathbf{M} \in \mathbb{R}^3 : |\mathbf{M}| = 1$ is the unit sphere), I_4 , the fourth pseudo-invariant, is the square of the stretch of a fiber in the direction $\mathbf{m} = \mathbf{F}\mathbf{M}$, i.e.
155 $I_4(\mathbf{M}) = \lambda^2(\mathbf{M}) = \mathbf{M} \cdot \mathbf{C}_S \mathbf{M}$, $k_1 > 0$ and $k_2 > 0$ are a stress-like material parameter and a dimensionless parameter, respectively, and \mathcal{H} is a Heaviside step function evaluated at $(I_4 - 1)$, thus ensuring fibers only engage under tensile stretches.

To capture the corresponding permeation of interstitial fluid, we define the seepage velocity $\mathbf{w}_{\text{FS}} = \mathbf{x}'_{\text{F}} - \mathbf{x}'_{\text{S}}$, i.e. the difference between the fluid phase \mathbf{x}'_{F} and the solid phase \mathbf{x}'_{S} .
160 We model the filtration velocity $n^{\text{F}} \mathbf{w}_{\text{FS}} = \mathbf{K}_{\text{F}}(-\text{grad } p + \rho^{\text{FR}} \mathbf{b})$, where \mathbf{K}_{F} is the anisotropic intrinsic permeability of the cartilage and \mathbf{b} is the body force per unit mass [48]. Considering that permeation of interstitial fluid is least restricted in the direction parallel to the fibers we formulate \mathbf{K}_{F} as [48, 49]

$$\mathbf{K}_{\text{F}} = \frac{k_{\text{OS}}}{4\pi} \left(\frac{n^{\text{F}}}{1 - n_{\text{OS}}^S} \right)^m \int_{\Omega} \frac{\rho(\mathbf{M})}{I_4(\mathbf{m})} \mathbf{m} \otimes \mathbf{m} \, d\Omega, \quad (11)$$

where k_{0S} is the Darcy permeability and m is a dimensionless parameter controlling the
 165 deformation dependence of the permeability [58].

2.2. Model formulation II: Signaling-pathways biochemical model of cartilage

We recently established a system of ordinary differential equations (ODEs) to describe
 the time evolution of “minimally essential” chemical, structural, and cellular species [46]. We
 briefly overview our full signaling pathways biochemical model and highlight two interactions
 170 with specialized coupling functions. The first coupling function $f_S(\sigma_i(\mathbf{x}), \tau)$, $i \in \{\text{sh}, 1\}$
 (taking either first principal stress or maximum shear stress as an argument, see §2.3.1)
 acts on the basal rate parameters, controlling mechanobiological responses based on local
 injurious or pathological mechanical stimuli. The second coupling function $f_A(O_2(\mathbf{x}), \tau)$
 (taking oxygen concentration as an argument, see §2.3.2) acts on the basal rate parameters,
 175 controlling production and degradation based on the local oxygen concentration.

Briefly, production of normal chondrocytes \hat{n}_c is proportional to the number of existing
 chondrocytes and is mediated by both local oxygen concentration and active growth
 factors \hat{c}_β [59]. Depletion of chondrocytes results from natural decay, phenotypic switching
 to hypertrophic chondrocytes regulated by growth factors \hat{c}_β , and apoptosis driven by
 180 pro-inflammatory cytokines \hat{c}_p [30, 60, 61]. Hypertrophic chondrocytes \hat{n}_{hc} , produced due
 to phenotypic switching of proliferated chondrocytes, degrade naturally (exponential decay).
 Injurious loading can cause living chondrocytes to become necrotic [62], denoted by \hat{n}_{nc} , and
 these similarly degrade naturally. We model the time evolution of normal, hypertrophic, and
 necrotic chondrocytes as

$$\frac{d\hat{n}_c}{d\tau} = [f_A(O_2)r_1^c + r_2^c\hat{c}_\beta]\hat{n}_c - [f_A(O_2)r_3^c + r_4^c\hat{c}_\beta + r_5^c\hat{c}_p]\hat{n}_c, \quad (12)$$

$$\frac{d\hat{n}_{hc}}{d\tau} = f_A(O_2)r_1^{hc}\hat{c}_\beta\hat{n}_c - f_A(O_2)r_2^{hc}\hat{n}_{hc}, \quad (13)$$

$$\frac{d\hat{n}_{nc}}{d\tau} = -f_A(O_2)r_1^{nc}\hat{n}_{nc}, \quad (14)$$

185 where r_1^c , r_2^c , r_3^c , r_4^c , r_5^c are the rate parameters for normal chondrocytes; r_1^{hc} , r_2^{hc} are the
 rate parameters for hypertrophic chondrocytes; and r_1^{nc} is the rate parameter for necrotic
 chondrocytes.

We model two different masses of type II collagen, i.e. functional or load-bearing collagen
 \hat{m}_{co}^{fn} and damaged collagen \hat{m}_{co}^{dm} which does not bear load. Normal chondrocytes \hat{n}_c

190 produce functional collagen $\hat{m}_{\text{co}}^{\text{fn}}$ and proteoglycan \hat{m}_{pg} , and active growth factors \hat{c}_β promote production [63, 64]. Collagen (both $\hat{m}_{\text{co}}^{\text{fn}}$ and $\hat{m}_{\text{co}}^{\text{dm}}$) and proteoglycan degrade naturally with collagenases \hat{c}_{ca} and aggrecanases \hat{c}_{ag} , respectively. Total collagen \hat{m}_{co} is the sum of $\hat{m}_{\text{co}}^{\text{fn}}$ and $\hat{m}_{\text{co}}^{\text{dm}}$. The metabolic activity function $f_{\text{A}}(\text{O}_2)$ acts on the basal rate parameters of the production of proteoglycan and collagen determining their rates of production. We model
 195 the time evolution of functional and damaged collagen, and proteoglycan as

$$\frac{d\hat{m}_{\text{co}}^{\text{fn}}}{d\tau} = [f_{\text{A}}(\text{O}_2)r_1^{\text{co}} + r_2^{\text{co}}\hat{c}_\beta]\hat{n}_{\text{c}} - r_3^{\text{co}}\hat{c}_{\text{ca}}\hat{m}_{\text{co}}^{\text{fn}}, \quad (15)$$

$$\frac{d\hat{m}_{\text{co}}^{\text{dm}}}{d\tau} = -r_4^{\text{co}}\hat{c}_{\text{ca}}\hat{m}_{\text{co}}^{\text{dm}}, \quad (16)$$

$$\frac{d\hat{m}_{\text{pg}}}{d\tau} = [f_{\text{A}}(\text{O}_2)r_1^{\text{pg}} + r_2^{\text{pg}}\hat{c}_\beta]\hat{n}_{\text{c}} - r_3^{\text{pg}}\hat{c}_{\text{ag}}\hat{m}_{\text{pg}}, \quad (17)$$

where r_1^{co} , r_2^{co} , r_3^{co} , r_4^{co} are the rate parameters for collagen and r_1^{pg} , r_2^{pg} , r_3^{pg} are the rate parameters for proteoglycan.

Normal chondrocytes \hat{n}_{c} express collagenases \hat{c}_{ca} (MMP-1, 3, 13, etc.) and aggrecanases \hat{c}_{ag} (ADAMTS-4, 5, etc.) within cartilage [65, 66]. Active pro-inflammatory cytokines
 200 \hat{c}_{p} promote production of these proteinases [67, 68], while active growth factors \hat{c}_β inhibit production [69]. Production of collagenases and aggrecanases further depends on local oxygen concentration. Hypertrophic cells \hat{n}_{hc} also express aggrecanases and collagenases [70]. Degradation of these proteinases results from natural decay and decay of inhibitory complex TIMP \hat{c}_{i} . We model the time evolution of collagenases and aggrecanases respectively

205 as

$$\frac{d\hat{c}_{\text{ca}}}{d\tau} = \left[\frac{f_{\text{A}}(\text{O}_2)r_1^{\text{ca}} + r_2^{\text{ca}}\hat{c}_{\text{p}}}{1 + r_3^{\text{ca}}\hat{c}_\beta} \right] \hat{n}_{\text{c}} + f_{\text{A}}(\text{O}_2)r_4^{\text{ca}}\hat{n}_{\text{hc}} - [r_5^{\text{ca}} + r_6^{\text{ca}}\hat{c}_{\text{i}}]\hat{c}_{\text{ca}}, \quad (18)$$

$$\frac{d\hat{c}_{\text{ag}}}{d\tau} = \left[\frac{f_{\text{A}}(\text{O}_2)r_1^{\text{ag}} + r_2^{\text{ag}}\hat{c}_{\text{p}}}{1 + r_3^{\text{ag}}\hat{c}_\beta} \right] \hat{n}_{\text{c}} + f_{\text{A}}(\text{O}_2)r_4^{\text{ag}}\hat{n}_{\text{hc}} - [r_5^{\text{ag}} + r_6^{\text{ag}}\hat{c}_{\text{i}}]\hat{c}_{\text{ag}}, \quad (19)$$

where r_1^{ca} , r_2^{ca} , r_3^{ca} , r_4^{ca} , r_5^{ca} , r_6^{ca} are the rate parameters for collagenases and r_1^{ag} , r_2^{ag} , r_3^{ag} , r_4^{ag} , r_5^{ag} , r_6^{ag} are the rate parameters for aggrecanases.

Normal chondrocytes \hat{n}_{c} produce TIMP \hat{c}_{i} , dependent on the oxygen concentration $f_{\text{A}}(\text{O}_2)$, and active growth factors \hat{c}_β upregulate production [69]. TIMP degrades by uptake
 210 from chondrocytes and natural decay with collagenases \hat{c}_{ca} and aggrecanases \hat{c}_{ag} [29]. We

model the time evolution of TIMP as

$$\frac{d\hat{c}_i}{d\tau} = [f_A(O_2)r_1^i + r_2^i\hat{c}_\beta]\hat{n}_c - \left[r_3^i\hat{n}_c + \frac{(r_4^i\hat{c}_{ca} + r_5^i\hat{c}_{ag})}{f_A(O_2)} \right] \hat{c}_i, \quad (20)$$

where $r_1^i, r_2^i, r_3^i, r_4^i, r_5^i$ are the rate parameters for TIMP. Due to the nonlinear term, we divide the rate parameters r_4^i and r_5^i by $f_A(O_2)$ to satisfy homeostatic balance at $\tau = 0$.

Normal chondrocytes \hat{n}_c produce latent growth factors $\hat{c}_{\ell\beta}$ (including transforming growth factors, TGF- β 1-3, activins; bone morphogenetic protein, BMP; and growth/differentiation factors, GDF) which are stored in the ECM and upregulated by active growth factors \hat{c}_β and dependent on oxygen concentration $f_A(O_2)$. Mechanical forces within cartilage, e.g. tension or shear, activate latent growth factors by breaking bonds between latency-associated peptides (LAPs) and latent TGF- β binding proteins (LTBPs) [61, 69, 71–73]. Hence, a portion of latent growth factors activate to active forms \hat{c}_β within chondrocytes under pathological mechanical stimuli ($f_S(\sigma_{sh}, \sigma_{sh,hom}^j) > 0$, see §2.3.1) [71, 72, 74]. Both latent and active growth factors degrade naturally. We model the time evolution of latent and active growth factors as

$$\frac{d\hat{c}_{\ell\beta}}{d\tau} = [f_A(O_2)r_1^{\ell\beta} + r_2^{\ell\beta}\hat{c}_\beta]\hat{n}_c - [r_3^{\ell\beta} + f_S(\sigma_{sh}, \sigma_{sh,hom}^j)r_4^{\ell\beta}]\hat{c}_{\ell\beta}, \quad (21)$$

$$\frac{d\hat{c}_\beta}{d\tau} = f_S(\sigma_{sh}, \sigma_{sh,hom}^j)r_1^\beta\hat{c}_{\ell\beta} - r_2^\beta\hat{c}_\beta, \quad (22)$$

where $r_1^{\ell\beta}, r_2^{\ell\beta}, r_3^{\ell\beta}$ are the rate parameters for latent growth factors; $r_4^{\ell\beta}$ is the rate parameter for conversion of latent to active growth factors; and r_1^β and r_2^β are the rate parameters of active growth factors.

Normal chondrocytes \hat{n}_c produce pro-inflammatory cytokines $\hat{c}_{\ell p}$ (including IL-1 β , NF- κ B, and TNF- α [28]) dependent on oxygen concentration $f_A(O_2)$. The active form of these cytokines \hat{c}_p promote greater production of latent forms [67, 68], while active growth factors \hat{c}_β inhibit production of latent pro-inflammatory cytokines [69]. Necrotic cells \hat{n}_{nc} also produce latent pro-inflammatory cytokines. A portion of latent pro-inflammatory cytokines $\hat{c}_{\ell p}$ activate to active pro-inflammatory cytokines \hat{c}_p under pathological mechanical stimuli ($f_S(\sigma_1, \sigma_{1,hom}^j) > 0$, see §2.3.1) [75–77]. Both latent and active pro-inflammatory cytokines degrade naturally. We model the time evolution of latent and active pro-inflammatory

235 cytokines as

$$\frac{d\hat{c}_{\ell\text{P}}}{d\tau} = \left[\frac{f_{\text{A}}(\text{O}_2)r_1^{\ell\text{P}} + r_2^{\ell\text{P}}\hat{c}_{\text{P}}}{1 + r_3^{\ell\text{P}}\hat{c}_{\beta}} \right] [1 + f_{\text{A}}(\text{O}_2)r_4^{\ell\text{P}}\hat{n}_{\text{nc}}]\hat{n}_{\text{c}} - [r_5^{\ell\text{P}} + f_{\text{S}}(\sigma_1, \sigma_{1,\text{hom}}^j)r_6^{\ell\text{P}}]\hat{c}_{\ell\text{P}}, \quad (23)$$

$$\frac{d\hat{c}_{\text{P}}}{d\tau} = f_{\text{S}}(\sigma_1, \sigma_{1,\text{hom}}^j)r_1^{\text{P}}\hat{c}_{\ell\text{P}} - r_2^{\text{P}}\hat{c}_{\text{P}}, \quad (24)$$

where $r_1^{\ell\text{P}}, r_2^{\ell\text{P}}, r_3^{\ell\text{P}}, r_4^{\ell\text{P}}, r_5^{\ell\text{P}}$ are the rate parameters for latent pro-inflammatory cytokines; $r_6^{\ell\text{P}}$ is the rate parameter for conversion of latent to active pro-inflammatory cytokines; and r_1^{P} and r_2^{P} are the rate parameter of active pro-inflammatory cytokines.

2.3. Model formulation III: Coupling functions

240 Coupling functions connect our signaling-pathways biochemical model to intra-cartilage mechanical and biochemical conditions, determined using finite element simulations or other means. We establish two such functions here, one for intra-tissue mechanics (including homeostatic adaption) and one for intra-tissue oxygen concentration.

2.3.1. Homeostasis and adaptation to mechanical stimuli

245 Normal physiological loading promotes chondrocytes to maintain homeostatic balance while injurious or pathological mechanical loading activate growth factors and pro-inflammatory cytokines [46, 67]. Briefly, following our previous work [46], we formulate mechanical stimuli functions $f_{\text{S}}(\sigma_i(\mathbf{x}), \tau)$ as

$$f_{\text{S}}(\sigma_i(\mathbf{x}), \tau) = \begin{cases} f^{\text{L,max}}, & \text{if } \sigma_i(\tau) \leq \sigma_{i,\text{hom}}^{\text{L}}(\tau) - w^{\text{L}} \\ f^{\text{L}}(\sigma_i(\tau), \sigma_{i,\text{hom}}^{\text{L}}(\tau), w^{\text{L}}), & \text{if } \sigma_{i,\text{hom}}^{\text{L}}(\tau) - w^{\text{L}} < \sigma_i(\tau) < \sigma_{i,\text{hom}}^{\text{L}}(\tau) \\ 0, & \text{if } \sigma_{i,\text{hom}}^{\text{L}}(\tau) \leq \sigma_i(\tau) \leq \sigma_{i,\text{hom}}^{\text{H}}(\tau) \\ f^{\text{H}}(\sigma_i(\tau), \sigma_{i,\text{hom}}^{\text{H}}(\tau), w^{\text{H}}), & \text{if } \sigma_{i,\text{hom}}^{\text{H}}(\tau) < \sigma_i(\tau) < \sigma_{i,\text{hom}}^{\text{H}}(\tau) + w^{\text{H}} \\ f^{\text{H,max}}, & \text{if } \sigma_i(\tau) \geq \sigma_{i,\text{hom}}^{\text{H}}(\tau) + w^{\text{H}} \end{cases}, \quad (25)$$

where f^{L} and f^{H} are sigmoidal functions, $\sigma_i(\tau)$ is the mechanical stimulus at evolution
250 time τ with $i \in \{\text{sh}, 1\}$, $\sigma_{i,\text{hom}}^{\text{L}}(\tau)$ and $\sigma_{i,\text{hom}}^{\text{H}}(\tau)$ represent low (L) and high (H) homeostatic thresholds of mechanical stimulus $\sigma_i(\tau)$ (subscript comma does not indicate differentiation). We activate growth factors using pathological maximum shear stresses, i.e. $f_{\text{S}}(\sigma_{\text{sh}}(\mathbf{x}), \tau)$ [71, 72, 74], while we activate pro-inflammatory cytokines using pathological first principal

stresses, i.e. $f_S(\sigma_1(\mathbf{x}), \tau)$ [75–77]. The constants $f^{L,\max} \in (0, 1]$ and $f^{H,\max} \in (0, 1]$ are
 255 maximum values of f_S under low and high pathological loading, and w^L and w^H are
 parameters controlling the width of the sigmoidal transition zones from physiological to
 pathological loading. We define $f_S(\sigma_{\text{sh}}(\mathbf{x}), \tau) = f_S(\sigma_1(\mathbf{x}), \tau) = 0$ under normal physiological
 loading, recognizing that active growth factors remain present to sustain cartilage health
 without inducing damage.

260 Chondrocytes adapt to injurious or pathological mechanical stimuli over time, to
 minimize deleterious longitudinal effects, by adapting to new homeostatic equilibriums over
 time [78, 79]. We model adaptation of homeostatic thresholds $\sigma_{i,\text{hom}}^L(\tau)$ and $\sigma_{i,\text{hom}}^H(\tau)$ as

$$\sigma_{i,\text{hom}}^L(\tau) = \begin{cases} \sigma_{i,\text{hom}}^{L,0}, & \text{if } \tau \leq \tau_{\text{del}}^L \\ \min \left[\sigma_{i,\text{hom}}^{L,0}, \left(\int_{\tau-\tau^L}^{\tau} \sigma_i(\tau) d\tau / \tau^L \right) \right], & \text{if } \tau > \tau_{\text{del}}^L \end{cases}, \quad (26)$$

$$\sigma_{i,\text{hom}}^H(\tau) = \begin{cases} \sigma_{i,\text{hom}}^{H,0}, & \text{if } \tau \leq \tau_{\text{del}}^H \\ \max \left[\sigma_{i,\text{hom}}^{H,0}, \left(\int_{\tau-\tau^H}^{\tau} \sigma_i(\tau) d\tau / \tau^H \right) \right], & \text{if } \tau > \tau_{\text{del}}^H \end{cases}, \quad (27)$$

where $\sigma_{i,\text{hom}}^{L,0}$ and $\sigma_{i,\text{hom}}^{H,0}$ are initial values of homeostatic thresholds for low and high
 265 pathological loading, respectively, τ_{del}^L and τ^L are time delay and averaging period for
 adaptation of the low (reduced loading) homeostatic threshold, and τ_{del}^H and τ^H are time
 delay and averaging period for adaptation of the high (overloading) homeostatic threshold.

2.3.2. Metabolic activity of chondrocytes

Chondrocytes *in vivo* live in hypoxic conditions: the concentration of oxygen is $\sim 10\%$ in
 270 the superficial zone (SZ) and $\sim 1\%$ in the deep zone (DZ) while the normoxic condition at
 sea level is $\sim 20\%$ [13, 30, 31]. We model the partial pressure of oxygen $f_{\text{O}_2}(z^*)$ as a function
 of the normalized cartilage thickness $z^* \in [0, 1]$ as

$$f_{\text{O}_2}(z^*) = \begin{cases} f_{\text{O}_2,\max} = 0.1, & \text{if } z^* = z_{\text{SZ}}^* \\ az^* + b, & \text{if } z^* = z_{\text{MZ}}^*, \\ f_{\text{O}_2,\min} = 0.01, & \text{if } z^* = z_{\text{DZ}}^* \end{cases}, \quad (28)$$

where, $z_{\text{SZ}}^* \in [0, 0.15]$, $z_{\text{MZ}}^* \in (0.15, 0.7]$, and $z_{\text{DZ}}^* \in (0.7, 1]$ represent the normalized thickness ranges of superficial (SZ), middle (MZ) and deep (DZ) zones, respectively [3]; and $a = -0.818$ and $b = 0.623$ are coefficients such that $f_{\text{O}_2}(z^*)$ that decreases linearly from SZ to DZ.

Experimental evidence suggests the concentration of available oxygen correlates positively with chondrocyte metabolism (in the presence of nutrients), i.e. greater production and degradation of constituents [31, 32]. We assume a linear relationship between metabolic activity and the partial pressure of oxygen and model the metabolic activity function as

$$f_{\text{A}}(\text{O}_2(\mathbf{x}), \tau) = 10f_{\text{O}_2}(z^*), \quad (29)$$

where $f_{\text{A}}(\text{O}_2(\mathbf{x}), \tau) \in [0, 1]$.

2.4. Algorithmic and numerical implementation

We implemented our chemo-mechano-biological framework within FEBio 4.2 (University of Utah, Salt Lake City, UT) [80] utilizing the standard forward solver to run iteratively, as detailed in Table 1. Initial iteration $i = 0$ starts with the

Table 1: **Algorithmic implementation of the chemo-mechano-biological (CMB) framework.**

1:	$i \leftarrow 0$	
2:	$\tau \leftarrow \tau^0, \mathbf{d}^0$	\triangleleft initialization
3:	$\mathbf{X}_{\text{initial}} \leftarrow \mathbf{X}^0$	
4:	while $i = 0$ or $\tau \leq \tau^{\text{max}}$ do	
5:	$\mathbf{X}_{\text{img}}^i \leftarrow \mathbf{X}_{\text{initial}}$	\triangleleft osmotic swelling
6:	$\mathbf{X}_{\text{bvp}}^i, \Delta\sigma \ll \epsilon$	\triangleleft solve boundary value problem, e.g. cyclic loading
7:	$\sigma_i^{\text{max}}, \text{O}_2 \rightarrow$ signaling – pathways model	\triangleleft apply stresses and O_2 to biochemical signaling pathways
8:	\hat{v}	\triangleleft calculate volume change
9:	$\mathbf{F}(\tau^i) = \mathbf{F}_{\text{S}}\mathbf{F}^{\text{E}}(\tau^i)$	\triangleleft apply growth to current deformation gradient
10:	Update \mathbf{d}^i	\triangleleft update material properties
11:	$\mathbf{X}_{\text{relax}}^i$	\triangleleft boundary value problem, no loading
12:	$i = i + 1$	
13:	$\mathbf{X}_{\text{initial}} \leftarrow \mathbf{X}_{\text{relax}}^i$	\triangleleft update nodal positions
14:	end while	

initial evolution time τ^0 and initial vector of model variables \mathbf{d}^0 considering tissue is healthy and in a stress-free, reference configuration \mathbf{X}^0 , and with $\mathbf{d}^i = \{\hat{n}_{\text{c}} \hat{n}_{\text{hc}} \hat{n}_{\text{nc}} \hat{m}_{\text{co}}^{\text{fn}} \hat{m}_{\text{co}}^{\text{dm}} \hat{m}_{\text{pg}} \hat{c}_{\text{ca}} \hat{c}_{\text{ag}} \hat{c}_{\text{i}} \hat{c}_{\ell\beta} \hat{c}_{\beta} \hat{c}_{\ell\text{p}} \hat{c}_{\text{p}} f_{\text{S}}(\sigma_{\text{sh}}) f_{\text{S}}(\sigma_1)\}^{\text{T}}$ evaluated at time τ . To begin each iteration, we osmotically prestress the stress-free, reference configuration

into an imaged configuration $\mathbf{X}_{\text{img}}^i$ (a pre-stressed reference configuration) to which we
 290 may apply chemical, mechanical, and/or biological loads. Given a specific boundary value
 problem (BVP), likely with cyclic loading (e.g. walking or running), we achieve a repeatable
 chemo-mechano-biological condition (e.g. the range of mechanical stresses during a loading
 cycle remains constant). We extract repeatable stress data from the BVP during the
 most extreme loading (maximum deformations) and pass them to the signaling-pathways
 295 biochemical model to evaluate the evolution of constituents. We calculate the total volume
 change \hat{v} summing up the structural constituents times their corresponding volume fractions,
 and update the material parameter vector \mathbf{d}^i . We relax cartilage to reabsorb exuded fluid
 and to grow or degrade following the volume change \hat{v} . We repeat the BVP starting with an
 updated reference configuration $\mathbf{X}_{\text{relax}}^i$. The simulation ends when the iteration reaches the
 300 maximum evolution time τ^{max} .

Numerically, we first establish the intra-cartilage distribution of mechanical stresses by
 solving a standard time-dependent FE analysis with FEBio (with time in seconds). We then
 establish the current state of chemical, mechanical, and biological constituents by solving the
 system of ODEs (12) - (24) using a backward-finite-difference Euler approach. We define the
 305 initial conditions for the normalized quantities \hat{n}_c , \hat{m}_{co} , \hat{m}_{pg} , as unity. However, we define
 the initial concentrations of chemical species equal to the values of the depth-dependent
 cellular activity function, i.e. $\hat{c}_{\text{ca}} = f_A(\text{O}_2(\mathbf{x}), \tau)$, $\hat{c}_{\text{ag}} = f_A(\text{O}_2(\mathbf{x}), \tau)$, $\hat{c}_i = f_A(\text{O}_2(\mathbf{x}), \tau)$,
 $\hat{c}_{\ell\beta} = f_A(\text{O}_2(\mathbf{x}), \tau)$, and $\hat{c}_{\ell\text{p}} = f_A(\text{O}_2(\mathbf{x}), \tau)$. Hypertrophic chondrocytes are generally not
 present in healthy cartilage and therefore we define \hat{n}_{hc} initially as zero. In health, we define
 310 the active chemical species \hat{c}_p and \hat{c}_β initially as zero since they are not activated unless
 cartilage undergoes pathological loading. Simulations start at zero months with cartilage
 in a healthy homeostatic condition, and pathological conditions begin when we start the
 simulations.

We verified the correct implementation of our system of ODEs (12) - (24), and its
 315 interactions with the biomechanical constitutive model of cartilage, within FEBio by
 comparison against our original implementation within MATLAB R2021b (The Mathworks,
 Natick, MA) [46], cf. Appendix A.

2.5. Model parameters

2.5.1. Biomechanical constitutive model of cartilage

320 We list the model parameters for the biomechanical constitutive model of cartilage (§2.1.2) in Table 2. We define the heterogeneous angular fiber density $\rho(\mathbf{M})$ based on diffusion tensor MRI data previously reported [48, 57].

Table 2: **Parameters for biomechanical constitutive model of cartilage.** Through-thickness material, compositional, and structural parameters for cartilage and corresponding units ([48], [49]). The parameter $z^* \in [0, 1]$ is the normalized tissue thickness, where zero refers to the articular surface and one refers to the interface with subchondral bone.

Parameter	Value	Unit	Equation
μ^S	0.23	MPa	(7), (8)
k_1, k_2	3, 8	MPa, –	(10)
$n_{0S}^S(z^*)$	$0.15 + 0.15(z^*)$	–	(6),(11)
$\nu^0(z^*)$	$0.43(z^*)^2 - 0.60(z^*) + 0.85$	–	(3),(4)
J_{cp}^S	$0.36 + 0.11(z^*)$	–	(9)
$k_{0S}(z^*)$	$[1 - 0.9(z^*)] \times 10^{-3}$	mm ⁴ /Ns	(11)
$m(z^*)$	$3 + 5.0(z^*)$	–	(11)
$c_{0S}^{fc}(z^*)$	$[1.0 + 2.6(z^*)] \times 10^{-7}, z^* \in [0, 0.5]$	mol/mm ³	(5),(6)
	$2.3 \times 10^{-7}, z^* \in (0.5, 0.75]$	mol/mm ³	
	$[4.4 - 2.8(z^*)] \times 10^{-7}, z^* \in (0.75, 1]$	mol/mm ³	
\bar{c}_m	1.5×10^{-7}	mol/mm ³	(5)

2.5.2. Signaling-pathways biochemical model of cartilage

325 We list the model parameters for our signaling-pathways biochemical model of cartilage (§2.2) in Tables 6 and 7 in Appendix B [46].

2.5.3. Homeostasis and adaptation to mechanical stimuli

We list the model parameters for homeostasis and adaptation to mechanical stimuli of cartilage that do not depend on the boundary value problem (§2.3.1) in Table 3. We establish the remaining required parameters (following §2.6.2) in §3.1, specifically Table 5.

320 2.6. Exercising the chemo-mechano-biological modeling framework

2.6.1. Boundary value problem

To exercise the framework, we simulated confined compression of a full-thickness cylindrical cartilage explant with radius of 1.5 mm and height of 2 mm in 3-D, Fig. 1.

Table 3: **Parameters for homeostasis and adaptation to mechanical stimuli.** Model parameters and corresponding units for cartilage that do not depend on the boundary value problem [46].

Parameter	Value	Unit	Equation
τ_{del}^L	0.5	month	(26)
τ_{del}^H	0.5	month	(27)
τ^L	15	month	(26)
τ^H	9	month	(27)

To reduce the computational expense, we modeled a one-degree slice of the cylindrical,

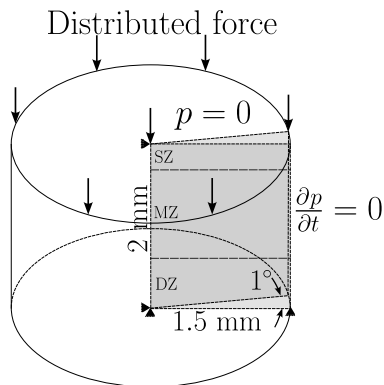


Figure 1: **Schematic illustration of boundary value problem representing cartilage explant undergoing cyclic, confined compression.** We used a one-degree slice of a cylindrical, full-thickness cartilage explant (radius and thickness equal 1.5 mm and 2 mm, respectively). We applied boundary conditions representing cyclic, confined compression via loading from a rigid permeable platen (not shown) to the articular surface. We divide the full thickness into three zones, i.e. superficial (SZ = 15%), middle (MZ = 55%), and deep (DZ = 30%) zones [3].

335 full-thickness cartilage explant meshed with 20 eight-node trilinear hexahedral elements. We established the accuracy of our simulation by refining the mesh until the displacement-time response of the top surface changed less than one percent upon subsequent refinements. On the bottom (bone interface) surface of the explant slice we set all displacement degrees of freedom, and fluid flux, i.e. $\partial p / \partial t = 0$, to zero. On the outer surface of the cylindrical slice
340 we set displacements normal to the surface, and fluid flux, to zero. On the two cutting planes defining symmetries we also set displacements normal to the surface, and fluid flux, to zero. On the top (articular) surface we applied time-dependent, cyclic compression at one Hz as a distributed force and allowed fluid to exude freely, i.e. $p = 0$.

To establish the magnitude of the total force distributed on the articular surface F of

345 our BVP we converted the compressive force acting inside an average human knee as [81]

$$F = M \left(\frac{a_s}{a_k} \right) m_b g, \quad (30)$$

where M is an activity-specific load multiplier [82], $a_s = (\pi r^2)/360 = 0.02 \text{ mm}^2$ is the contact area of the one-degree slice of specimen ($r = 1.5 \text{ mm}$), $a_k = 958 \text{ mm}^2$ is the average contact area within a human knee, $m_b = 70.8 \text{ kg}$ is the average human body mass [83], and $g = 9.81 \text{ m/s}^2$ is the gravitational constant.

350 2.6.2. Validation and calibration

We first completed one validation study to establish the physiological relevance of our BVP. We simulated cyclic, confined compression of our cylindrical explant mimicking normal walking at one Hertz, using activity-specific load multiplier $M = 4$ [82] in (30). We compared our simulation results for 60 minutes of walking to corresponding experimental results from
355 Paranjape et al. [84].

To determine the model parameters for homeostasis and adaptation to mechanical stimuli we first simulated cyclic, confined compression using activity-specific load multipliers $M = 4$ and $M = 8$ for normal walking and running, respectively [82] and extracted the corresponding zone-specific maximum shear and first principal stresses as homeostatic thresholds.

360 2.6.3. Numerical studies of cartilage degeneration during cyclic overloading

We completed three numerical studies to exercise our 3-D, coupled chemo-mechano-biological modeling framework for cartilage undergoing overloading ($M = 12$) for $\tau = 24$ months. At each month τ we simulated 2000 seconds of mechanical loading to establish a repeatable mechanical response prior to
365 updating the signaling-pathways biochemical model establishing the intermediate chemo-mechano-biological conditions for the next month, cf. §2.4.

Study 1: Cartilage evolving with spatially constant homeostatic values, without homeostatic adaptation, and with spatially constant metabolic activity.

In this simulation we consider a special case with spatially constant homeostatic values
370 (using the peak values from Table 5), without homeostatic adaptation (not using (26) and (27)), and with spatially constant metabolic activity (not using (28) and (29), but setting $f_A(\text{O}_2(\mathbf{x}), \tau) = 1$).

Study 2: Cartilage evolving with depth-dependent homeostatic values, with homeostatic adaptation, and with spatially constant metabolic activity. In this simulation we consider a special case with depth-dependent homeostatic values (using Table 5), with homeostatic adaptation (using (26) and (27)), and with spatially constant metabolic activity (not using (28) and (29), but setting $f_A(\text{O}_2(\mathbf{x}), \tau) = 1$).

Study 3: Cartilage evolving with depth-dependent homeostatic values, with depth-dependent metabolic activity, and with depth-dependent homeostatic adaptation. In this simulation we consider a special case employing the full heterogeneity available within our framework with depth-dependent homeostatic values (using Table 5), with homeostatic adaptation (using (26) and (27)), and with depth-dependent metabolic activity (using (28) and (29)).

For each study, we first report the intra-tissue mechanics of cartilage as they evolve over 24 months, specifically the average evolution within the SZ, MZ, and DZ. We then report the evolution of cellular, structural, and chemical constituents following Table 4 (a reference for plotting variables provided in the results), again specifically the average evolution within the SZ, MZ, and DZ. We did not model damage in any of the studies, thus

Table 4: **Plotting order for cellular, structural, and chemical constituents.** Symbols and definitions.

Number	Variable	Definition
(a)	\hat{h}	Thickness of cartilage
(b)	\hat{c}_i	Concentration of TIMPs
(c)	\hat{n}_c	Normalized density of living chondrocytes
(d)	\hat{n}_{hc}	Normalized density of hypertrophic chondrocytes
(e)	\hat{m}_{co}	Normalized density of collagen including functional and damaged
(f)	\hat{m}_{pg}	Normalized density of proteoglycan (PG)
(g)	\hat{c}_{ca}	Concentration of collagenases (MMPs)
(h)	\hat{c}_{ag}	Concentration of aggrecanases (ADAMTSs)
(i)	$\hat{c}_{\ell\beta}$	Concentration of latent growth factors
(j)	$\hat{c}_{\ell p}$	Concentration of latent pro-inflammatory cytokines
(k)	\hat{c}_{β}	Concentration of active growth factors
(l)	\hat{c}_p	Concentration of active pro-inflammatory cytokines

we excluded damaged collagen (16) and necrotic chondrocytes (14). Finally, we show the through-thickness evolution of key variables within the cross-section of the cartilage explant for 0, 6, 12, 18, and 24 months.

3. Results

3.1. Validation and calibration

To ensure the physiological relevance of our BVP we simulated cyclic, confined
395 compression of our cylindrical explant mimicking normal level walking, and predicted the
accumulation of compressive creep strain over 60 minutes. We compared our simulation
results for level walking with compressive strain measured *in-vivo* [84], see Fig. 2.

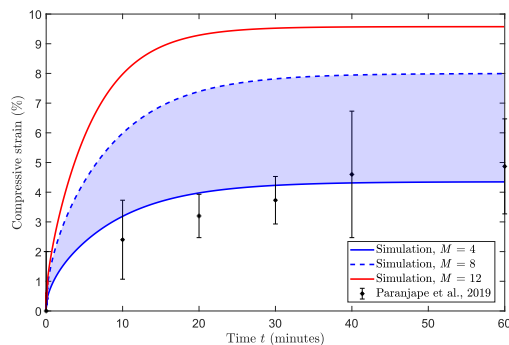


Figure 2: **Simulation results predict compressive strain measured *in-vivo* during walking.** We validated our BVP (cyclic, confined compression mimicking walking) against direct *in-vivo*, experimental measurements of accumulated compressive strain during walking. The solid blue curve presents the simulation result of a confined compression test using our constitutive model considering level walking, defined by the activity-specific load multiplier $M = 4$ [82]. The dashed blue curve presents the corresponding simulation result considering running, load multiplier $M = 8$, such that the blue shaded region encompasses normal physiological loading (maintaining homeostatic balance). The solid red curve presents the corresponding simulation result considering overloading, load multiplier $M = 12$. The simulation result for walking provides a good fit to experimental data from Paranjape et al. [84] who measured the compressive strains (mean, 95% confidence interval) during normal walking using magnetic resonance imaging at five time points over 60 minutes.

To calibrate our CMB framework for this specific BVP we simulated cyclic, confined
400 compression using activity-specific load multipliers $M = 4$ and $M = 8$ for normal walking
(low threshold L) and running (high threshold H), respectively [82]. We list the model
parameters for homeostasis and adaptation to mechanical stimuli of cartilage (§2.3.1) in
Table 5.

Table 5: **Parameters for homeostasis and adaptation to mechanical stimuli.** Through-thickness model parameters for cartilage and corresponding units [46]. The parameter $z^* \in [0, 1]$ is the normalized tissue thickness, where zero refers to the articular surface and one refers to the interface with subchondral bone, and where $z_{SZ}^* \in [0, 0.15]$, $z_{MZ}^* \in (0.15, 0.7]$, and $z_{DZ}^* \in (0.7, 1]$ represent the normalized thickness ranges of SZ, MZ and DZ, respectively [3].

Parameter	Value	Unit
$\sigma_{sh,hom}^{L,0}(z_{SZ}^*)$	3.439×10^{-3}	MPa
$\sigma_{sh,hom}^{L,0}(z_{MZ}^*)$	3.304×10^{-3}	MPa
$\sigma_{sh,hom}^{L,0}(z_{DZ}^*)$	3.294×10^{-3}	MPa
$\sigma_{sh,hom}^{H,0}(z_{SZ}^*)$	6.509×10^{-3}	MPa
$\sigma_{sh,hom}^{H,0}(z_{MZ}^*)$	6.241×10^{-3}	MPa
$\sigma_{sh,hom}^{H,0}(z_{DZ}^*)$	6.192×10^{-3}	MPa
$\sigma_{1,hom}^{L,0}(z_{SZ}^*)$	1.822	MPa
$\sigma_{1,hom}^{L,0}(z_{MZ}^*)$	1.752	MPa
$\sigma_{1,hom}^{L,0}(z_{DZ}^*)$	1.753	MPa
$\sigma_{1,hom}^{H,0}(z_{SZ}^*)$	3.641	MPa
$\sigma_{1,hom}^{H,0}(z_{MZ}^*)$	3.492	MPa
$\sigma_{1,hom}^{H,0}(z_{DZ}^*)$	3.496	MPa

3.2. Study 1: Cartilage evolving with spatially constant homeostatic values, without homeostatic adaptation, and with spatially constant metabolic activity

405 In this study, we simulate the evolution of cartilage during cyclic overloading, considering cells have a spatially constant homeostatic values, i.e., a constant homeostatic value through the thickness, and this homeostatic value does not evolve over time. We also exclude the effect of depth-dependent metabolic activity by specifying $f_A(O_2(\mathbf{x}), \tau) = 1$.

In Fig. 3 we show the time evolution of intra-tissue mechanics (along with homeostatic 410 thresholds) and of the mechanical stimulus functions that couple the mechanical model to the signaling-pathways biochemical model. Initially, when $\tau < 0$, cartilage receives physiological loading and the shear stresses σ_{sh} and first principal stresses σ_1 are within the homeostatic ranges (cf. Table 5) in all zones (Figs. 3(a), (b)). Once overloading begins at $\tau = 0$, σ_{sh} and σ_1 rise above the homeostatic thresholds, thus causing the mechanical stimuli $f_S(\sigma_{sh}) > 0$ and $f_S(\sigma_1) > 0$. Since the homeostatic values do not adapt over time, the mechanical stimuli 415 (both $f_S(\sigma_{sh})$ and $f_S(\sigma_1) \approx 0.6$) stay elevated (Figs. 3(c), (d)) for the entire simulation. We also observe that the fluid pressure decays over time as cartilage thins (Fig. 3(e)) while the porosity increases [85, 86] and becomes more uniform (Fig. 3(f)).

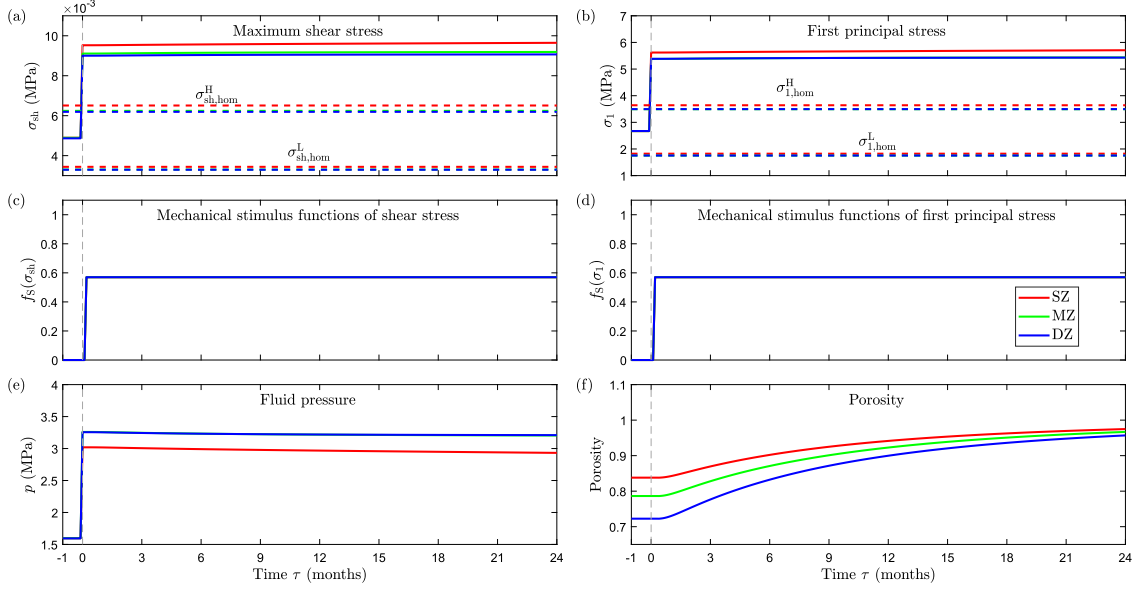


Figure 3: **Intra-tissue mechanics within cartilage evolving with spatially constant homeostatic values, without homeostatic adaptation, and with spatially constant metabolic activity.** Red, green, and blue curves represent the mean values of corresponding plot variables in superficial (SZ), middle (MZ), and deep (DZ) zones, respectively. Time $\tau < 0$ months represents healthy homeostasis. Specifically: (a) maximum shear stresses σ_{sh} , (b) first principal stresses σ_1 , (c) mechanical stimulus functions of shear stress $f_S(\sigma_{sh})$, (d) mechanical stimulus functions of first principal stress $f_S(\sigma_1)$, (e) fluid pressures p , and (f) porosities.

In Fig. 4 we show the time evolution of key constituents, following Table 4, during cyclic
420 overloading. The elevated mechanical stimuli (Figs. 3(c), (d)) activate latent growth factors
and pro-inflammatory cytokines (Figs. 4(k), (l)), which upregulate their latent forms (Figs.
10(i) and (j)) homogeneously. Activated growth factors and cytokines feed back to their
latent forms (Figs. 10(i) and (j)) and promote production. The activated pro-inflammatory
cytokines upregulate collagenases and aggrecanases (Figs. 4(g), (h)), which peak ($\hat{c}_{ca} \approx 30$
425 and $\hat{c}_{ag} \approx 10$) in approximately two months. Collagenases and aggrecanases degrade collagen
and proteoglycan (Figs. 4(e), (f)), which cause continuous loss of cartilage thickness (Fig.
4(a)). Over 24 months cartilage loses approximately 27% of its initial thickness and has
not stabilized. Activated pro-inflammatory cytokines also contribute to cell death (12)
and we observe a decrease in living chondrocytes (Fig. 4(c)). Activated growth factors
430 also promote production of TIMP (20) (which increases after a sharp loss, Fig. 4(b)),
chondrocyte proliferation (12), and production of collagen (15) and proteoglycan (17). Some

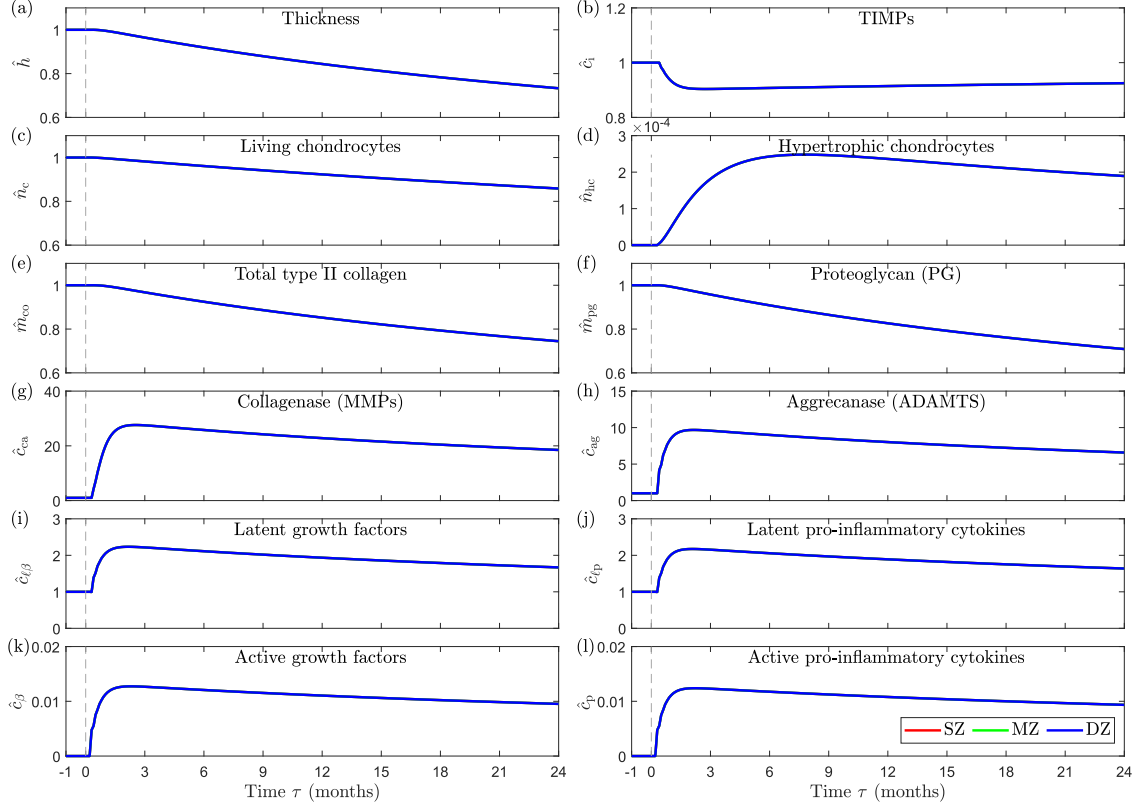


Figure 4: **Key constituents within cartilage evolving with spatially constant homeostatic values, without homeostatic adaptation, and with spatially constant metabolic activity.** Red, green, and blue curves represent the mean values of corresponding plot variables in superficial (SZ), middle (MZ), and deep (DZ) zones, respectively. Time $\tau < 0$ months represents healthy homeostasis. Overloading begins at $\tau = 0$ and causes activation of growth factors (21) and pro-inflammatory cytokines (23). Activated cytokines upregulate collagenases and aggrecanases, and promote further increase in production of latent cytokines that eventually convert to active forms. Upregulated collagenases and aggrecanases degrade collagen and proteoglycan, respectively, which presents as homogeneous thinning of cartilage. See Table 4 for a description of the variables.

proliferated chondrocytes become hypertrophic (Fig. 4(d)). The evolution of key constituents is homogeneous through the thickness, i.e. in the SZ, MZ, and DZ.

In Fig. 5 we show the evolution of normalized volume, collagen, proteoglycan, and chondrocytes at 0, 6, 12, 18, and 24 months on a full-thickness cross-section of the cartilage explant. Over 24 months we observe loss of normalized volume, collagen, proteoglycan, and living chondrocytes (Figs. 5(a) - (d)) which all progress homogeneously through the thickness, i.e. SZ, MZ and DZ.

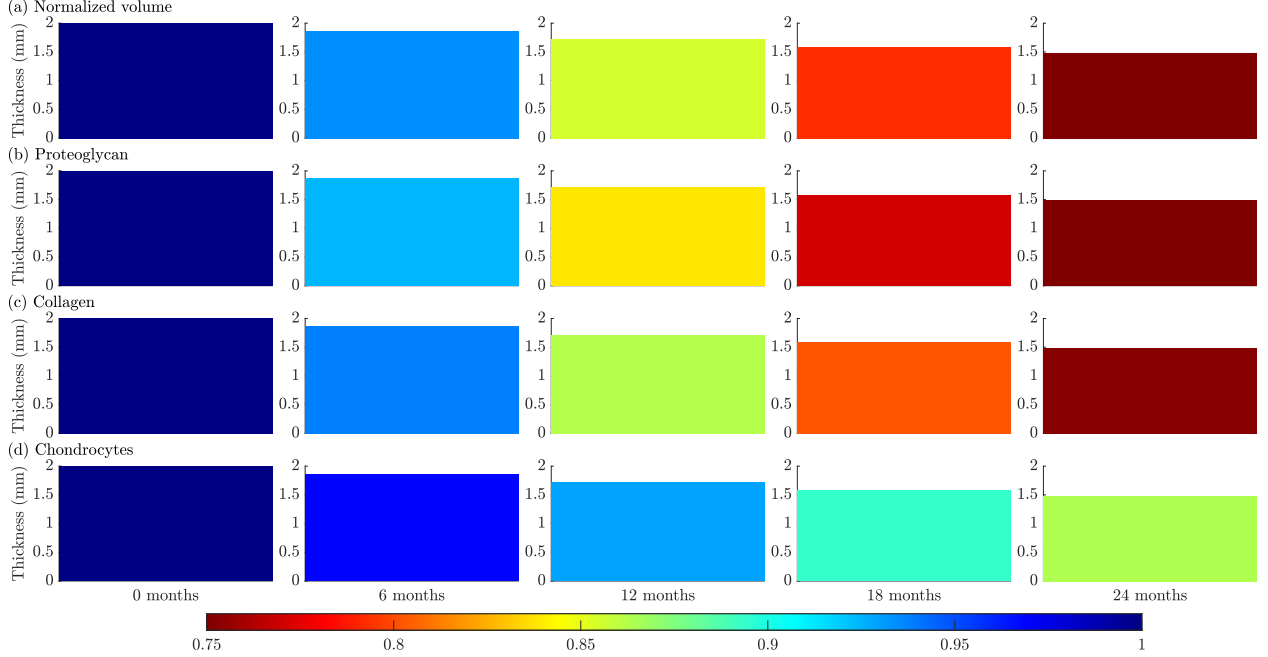


Figure 5: **Full-thickness cross-section of cartilage evolving with spatially constant homeostatic values, without homeostatic adaptation, and with spatially constant metabolic activity.** Cartilage evolves from healthy (0 month) to progressively degenerated in 6, 12, 18, and 24 months and loses approximately 27% of its initial thickness. Specifically, shown with a normalized scale: (a) normalized volume (\hat{v}) or thickness (\hat{h}), (b) proteoglycan (\hat{m}_{pg}), (c) collagen (\hat{m}_{co}), and (d) living chondrocytes (\hat{n}_c). N.B. Normalized volume is the mass-averaged sum of proteoglycan and collagen, cf. (4).

3.3. Study 2: Cartilage evolving with depth-dependent homeostatic values, with homeostatic adaptation, and with spatially constant metabolic activity

In this study, we simulate the evolution of cartilage during cyclic overloading, considering cells have depth-dependent homeostatic values, i.e. homeostatic values depend on the thickness location z^* , and these homeostatic values evolve over time. We also exclude the effect of depth-dependent metabolic activity by specifying $f_A(O_2(\mathbf{x}), \tau) = 1$.

In Fig. 6 we show the time evolution of intra-tissue mechanics (along with homeostatic thresholds) and of the mechanical stimulus functions. Similar to Study 1 (cf. §3.2), once overloading begins at $\tau = 0$ σ_{sh} and σ_1 rise above the homeostatic thresholds (Fig. 6(a) and (b)), thus causing the mechanical stimuli $f_S(\sigma_{sh}) > 0$ and $f_S(\sigma_1) > 0$. Since the homeostatic values adapt over time, the mechanical stimulus functions ($f_S(\sigma_{sh})$ and $f_S(\sigma_1)$) adapt to match the pathological stresses in all zones and over 9 months (Figs. 6(c), (d)). As a result, $f_S(\sigma_{sh})$ and $f_S(\sigma_1)$ return to zero once $\sigma_{sh, hom}^H$ and $\sigma_{1, hom}^H$ match the current stresses σ_{sh} and

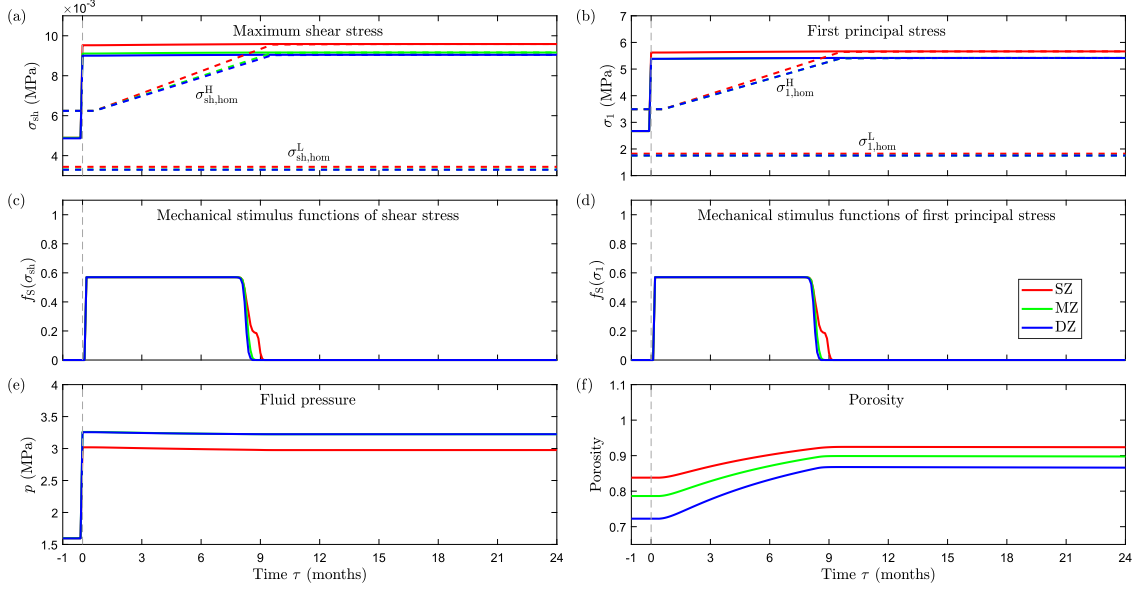


Figure 6: **Intra-tissue mechanics within cartilage evolving with depth-dependent homeostatic values, with homeostatic adaptation, and with spatially constant metabolic activity.** Red, green and blue curves represent the mean values of corresponding plot variables in superficial (SZ), middle (MZ), and deep (DZ) zones, respectively. Specifically: (a) maximum shear stresses σ_{sh} , (b) first principal stresses σ_1 , (c) mechanical stimulus functions of shear stress $f_S(\sigma_{sh})$, (d) mechanical stimulus functions of first principal stress $f_S(\sigma_1)$, (e) fluid pressures p , and (f) porosities.

σ_1 , respectively. We also observe that the fluid pressure decays over time as cartilage thins (Fig. 6(e)) while the porosity increases [85, 86] and becomes more uniform (Fig. 6(f)).

In Fig. 7 we show the time evolution of key constituents, following Table 4, during cyclic overloading. Similar to Study 1 (cf. §3.2), the elevated mechanical stimuli (Figs. 6(a), (b)) activate latent growth factors and pro-inflammatory cytokines (Figs. 7(k), (l)), which upregulate their latent forms (Figs. 7(i) and (j)) (with slight heterogeneity). Activated growth factors and cytokines feed back to their latent forms (Figs. 7(i) and (j)) and promote production. The activated pro-inflammatory cytokines upregulate collagenases and aggrecanases (Figs. 7(g), (h)), which peak (again $\hat{c}_{ca} \approx 30$ and $\hat{c}_{ag} \approx 10$) in approximately two months. Once \hat{c}_{lp} returns to zero in nine months \hat{c}_{ca} and \hat{c}_{ag} return to their basal levels. Collagenases and aggrecanases degrade collagen and proteoglycan (Figs. 7(e), (f)) until the normalized quantities reach equilibrium after nine months. Consequently, cartilage loses approximately 11% of its initial thickness after nine months and then stabilizes (Fig. 7(a)). Activated pro-inflammatory cytokines contribute to cell death and we observe a decrease in

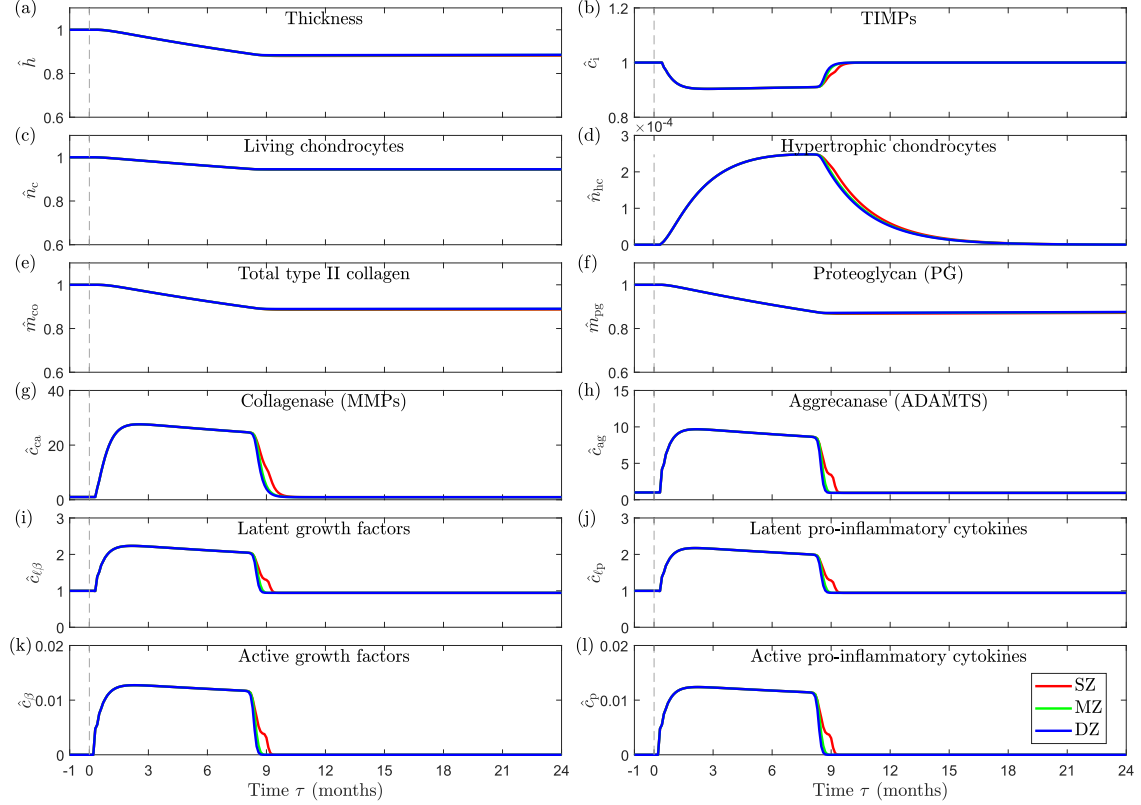


Figure 7: **Key constituents within cartilage evolving with depth-dependent homeostatic values, with homeostatic adaptation, and with spatially constant metabolic activity.** Red, green and blue curves represent the mean values of corresponding plot variables in superficial (SZ), middle (MZ), and deep (DZ) zones, respectively. Time $\tau < 0$ months represents healthy homeostasis. Overloading begins at $\tau = 0$ and causes activation of growth factors (21) and pro-inflammatory cytokines (23). Activated cytokines upregulate collagenases and aggrecanases, and promote further increase in production of latent cytokines that eventually convert to active forms. Upregulated collagenases and aggrecanases degrade collagen and proteoglycan, respectively, which presents as homogeneous thinning of cartilage. See Table 4 for a description of the variables.

living chondrocytes (Fig. 7(c)). Activated growth factors also promote production of TIMP (which increases after a sharp loss, Fig. 7(b)), chondrocyte proliferation, and production of collagen and proteoglycan. Some proliferated chondrocytes become hypertrophic (Fig. 7(d)). Although we considered depth-dependent homeostatic values with adaptation, the evolution of key constituents remains nearly homogeneous through the thickness, i.e. in the SZ, MZ, and DZ.

In Fig. 8 we show the evolution of normalized volume, collagen, proteoglycan, and

chondrocytes at 0, 6, 12, 18 and 24 months on a full-thickness cross-section of the cartilage explant. Over 24 months we observe loss of normalized volume, collagen, proteoglycan,

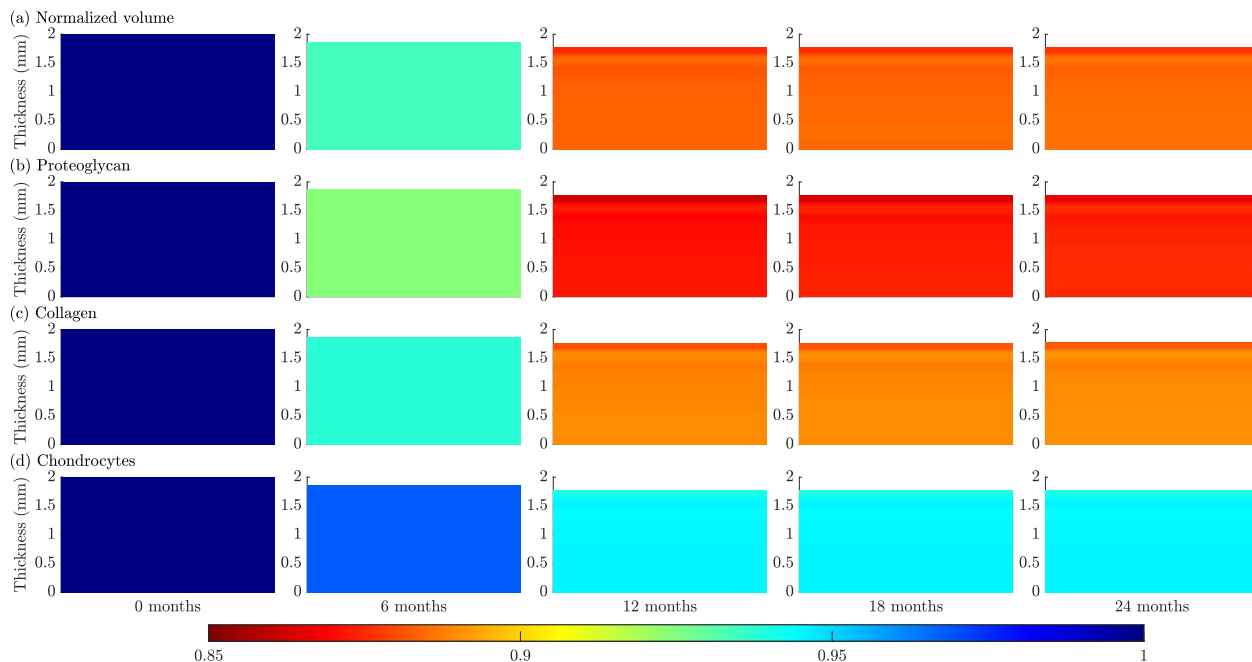


Figure 8: **Full-thickness cross-section of cartilage evolving with depth-dependent homeostatic values, with homeostatic adaptation, and with spatially constant metabolic activity.** Cartilage evolves from healthy (0 month) to progressively degenerated in 6, 12, 18, and 24 months and loses approximately 11% of its initial thickness. Specifically, shown with a normalized scale: (a) normalized volume, (b) proteoglycan, (c) collagen, and (d) living chondrocytes.

475 and living chondrocytes (Figs. 8(a) - (d)). While some of these constituents progress heterogeneously, they all stabilize after 9 to twelve months to present homogeneity through the thickness, i.e. SZ, MZ and DZ.

3.4. Study 3: Cartilage evolving with depth-dependent homeostatic values, with depth-dependent metabolic activity, and with depth-dependent homeostatic adaptation

480 In this study, we simulate the evolution of cartilage during cyclic overloading, considering cells have a depth-dependent homeostatic values, i.e. homeostatic value depend on the thickness location z^* , and these homeostatic values evolve over time. We also include the effect of depth-dependent metabolic activity by specifying $f_A(O_2(\mathbf{x}), \tau) = 1$ in SZ, $0.1 \leq f_A(O_2(\mathbf{x}), \tau) \leq 1$ in MZ, and $f_A(O_2(\mathbf{x}), \tau) = 0.1$ in DZ.

In Fig. 9 we show the time evolution of intra-tissue mechanics (along with homeostatic thresholds) and of the mechanical stimulus functions. Similar to Studies 1 and 2 (cf. §3.2 and

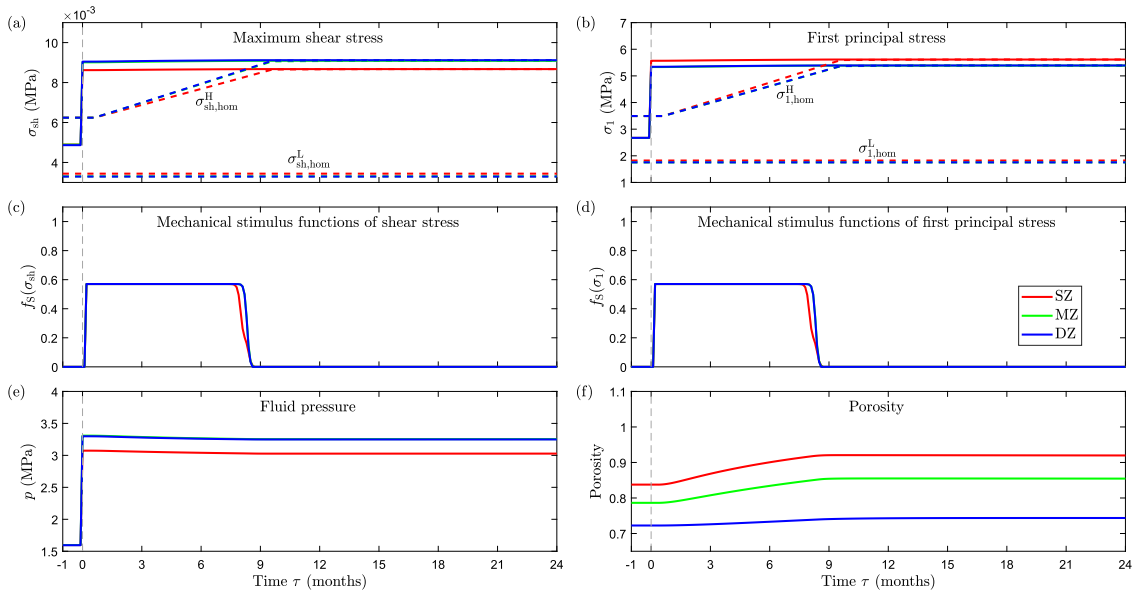


Figure 9: **Intra-tissue mechanics within cartilage evolving with depth-dependent homeostatic values, with depth-dependent metabolic activity, and with depth-dependent homeostatic adaptation.** Red, green, and blue curves represent the mean values of corresponding plot variables in superficial (SZ), middle (MZ), and deep (DZ) zones, respectively. Time $\tau < 0$ months represents healthy homeostasis. Specifically: (a) maximum shear stresses σ_{sh} , (b) first principal stresses σ_1 , (c) mechanical stimulus functions of shear stress $f_S(\sigma_{sh})$, (d) mechanical stimulus functions of first principal stress $f_S(\sigma_1)$, (e) fluid pressures p , and (f) porosities.

§3.3), once overloading begins at $\tau = 0$ σ_{sh} and σ_1 rise above the homeostatic thresholds (Fig. 9(a) and (b)), thus causing the mechanical stimuli $f_S(\sigma_{sh}) > 0$ and $f_S(\sigma_1) > 0$. Since the homeostatic values adapt over time, the mechanical stimulus functions ($f_S(\sigma_{sh})$ and $f_S(\sigma_1)$) adapt to match the pathological stresses in all zones and over 9 months (Figs. 6(c), (d)). As a result, $f_S(\sigma_{sh})$ and $f_S(\sigma_1)$ return to zero once $\sigma_{sh, hom}^H$ and $\sigma_{1, hom}^H$ match the current stresses σ_{sh} and σ_1 , respectively. We also observe that the fluid pressure decays over time as cartilage thins (Fig. 6(e)) while the porosity increases [85, 86] and becomes less uniform (Fig. 6(f)).

In Fig. 10 we show the time evolution of key constituents, following Table 4, during cyclic overloading. Similar to Studies 1 and 2, the elevated mechanical stimuli (Figs. 9(a), (b)) activate latent growth factors and pro-inflammatory cytokines (Figs. 10(k), (l)), which upregulate their latent forms (Figs. 10(i) and (j)) with strong heterogeneity though

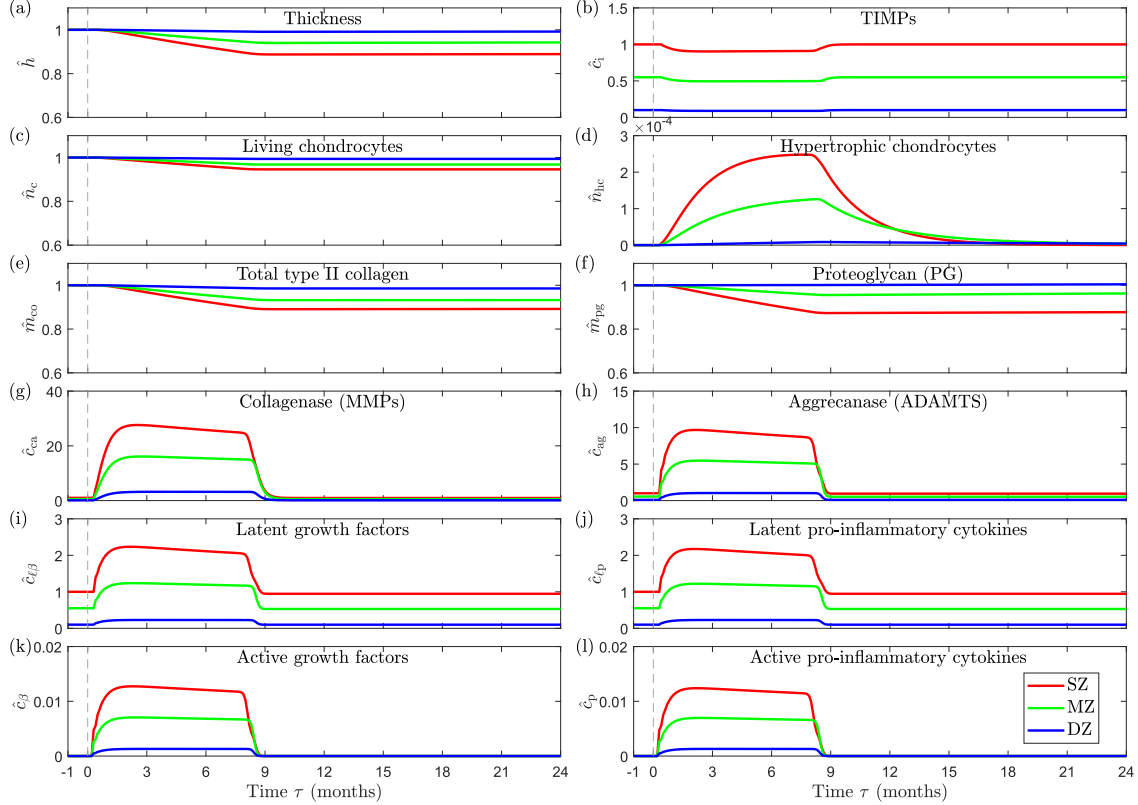


Figure 10: **Key constituents within cartilage evolving with depth-dependent homeostatic values, with depth-dependent metabolic activity, and with depth-dependent homeostatic adaptation.** Red, green and blue curves represent the mean values of corresponding plot variables in superficial (SZ), middle (MZ), and deep (DZ) zones, respectively. Time $\tau < 0$ months represents healthy homeostasis. Overloading begins at $\tau = 0$ and causes activation of growth factors (21) and pro-inflammatory cytokines (23). Activated cytokines upregulate collagenases and aggrecanases, and promote further increase in production of latent cytokines that eventually convert to active forms. Upregulated collagenases and aggrecanases degrade collagen and proteoglycan, respectively, which presents as heterogeneous thinning of cartilage, most pronounced within the SZ followed by the MZ. See Table 4 for a description of the variables.

the SZ, MZ, and DZ. Following the metabolic activity function $f_A(O_2(\mathbf{x}), \tau)$ production is approximately 10–fold higher in the SZ versus DZ. The activated pro-inflammatory cytokines upregulate collagenases and aggrecanases in all zones (Figs. 10(g), (h)). Both collagenases and aggrecanases peak in approximately two months ($\hat{c}_{ca} \approx 27, 16, \text{ and } 3$, and $\hat{c}_{ag} \approx 10, 5, \text{ and } 1$, in the SZ, MZ and DZ respectively). Once \hat{c}_{lp} returns to zero in nine months \hat{c}_{ca} and \hat{c}_{ag} return to their basal levels. Collagenases and aggrecanases degrade collagen and proteoglycan (Figs. 10(e), (f)) until the normalized quantities reach equilibrium after

505 nine months. Consequently, the SZ, MZ, and DZ lose approximately 12%, 7%, and 2% of their original thicknesses. Cumulatively, cartilage loses approximately 10% of its initial thickness after nine months and then stabilizes (Fig. 10(a)). Activated pro-inflammatory cytokines also contribute to cell death and we observe a decrease in living chondrocytes (Fig. 10(c)). Activated growth factors also promote production of TIMP (which increases after an initial loss, Fig. 10(b)), chondrocyte proliferation, and production of collagen and proteoglycan. Some proliferated chondrocytes become hypertrophic (Fig. 10(d)). We considered depth-dependent homeostatic values with adaptation and depth-dependent metabolic activity and the evolution of key constituents presented strong heterogeneity through the thickness, i.e. in the SZ, MZ, and DZ.

515 In Fig. 11 we show the evolution of normalized volume, collagen, proteoglycan, and chondrocytes at 0, 6, 12, 18 and 24 months on a full-thickness cross-section of the cartilage explant. Over 24 months we observe loss of normalized volume, collagen, proteoglycan, and

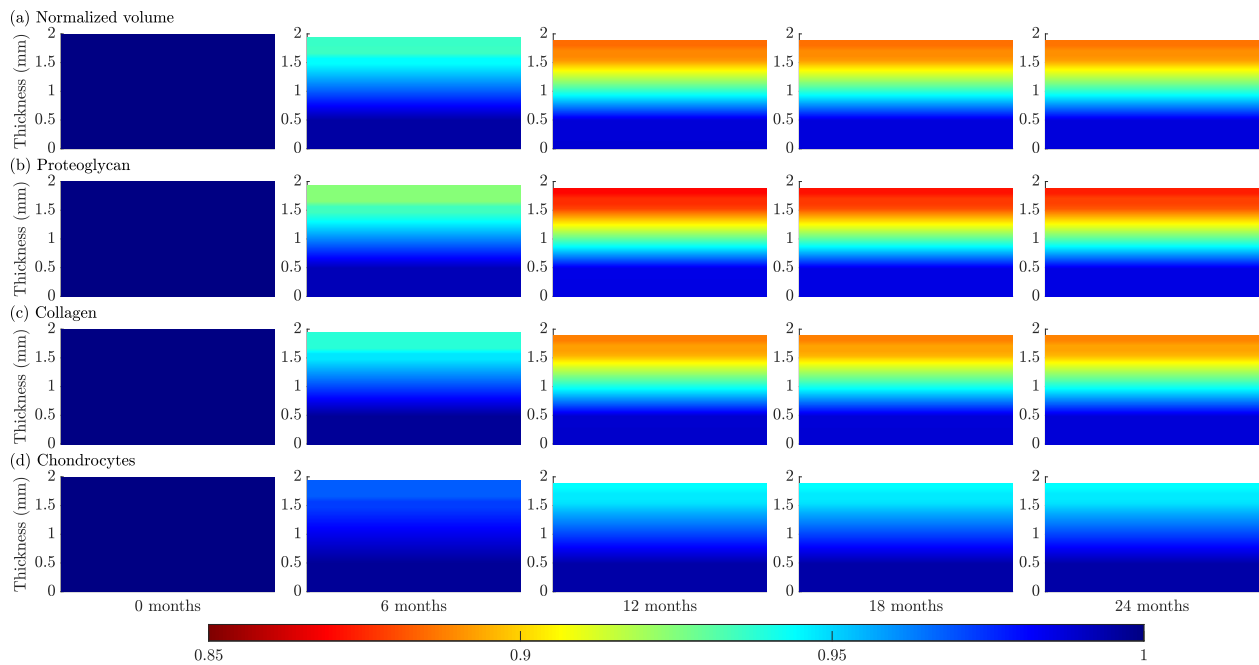


Figure 11: **Full-thickness cross-section of cartilage evolving with depth-dependent homeostatic values, with depth-dependent metabolic activity, and with depth-dependent homeostatic adaptation.** Cartilage evolves from healthy (0 month) to progressively degenerated in 6, 12, 18, and 24 months and loses approximately 10% of its initial thickness (heterogeneous losses of 12%, 7%, and 2% within the superficial, middle, and deep zones). Specifically, shown with a normalized scale: (a) normalized volume, (b) proteoglycan, (c) collagen, and (d) living chondrocytes.

living chondrocytes (Figs. 11(a) - (d)). All of these constituents progress heterogeneously, and they stabilize after 9 to twelve months to present strong heterogeneity through the thickness with the greatest degeneration in the SZ.

520 4. Discussion

We established a new modeling framework within 3-D biphasic FEs that includes time-dependent, chemo-mechano-biologically induced turnover of key constituents within cartilage resulting from biochemical, mechanical, and/or biological activity. FE analyses have previously been leveraged to model mechanoadaptation of tissues, e.g. arteries and bones
525 [87, 88], many with phenomenological approaches. Our novel computational framework is the first to fully integrate a nonlinear, large-strain constitutive model for the biphasic mechanics of cartilage with a signaling-pathways biochemical model of cartilage which drives growth-and-remodeling, and which feeds back to alter the mechanics. In formulating our signaling-pathways biochemical model we included the “minimally essential,” yet still
530 complex, chemical and mechanobiological mechanisms within cartilage.

The biological complexity of cartilage led us to formulate a simplified model capturing minimally essential mechanisms within a flexible and expandable framework. Thus, we defined the overall interactions among mechanical stimuli and biological/biochemical constituents, namely chondrocytes, collagenases, aggrecanases, TIMP, growth factors, and
535 pro-inflammatory cytokines, and their combined action on cartilage degeneration (specifically collagens and proteoglycans). We also estimated the required rate parameters based on available experimental data [46]. We further extended our prior work by establishing coupling functions, i.e. functions that couple intra-tissue conditions or results from multi-physics simulations, to inform our signaling-pathways biochemical model. In our prior work we
540 included adapting mechanical stimuli functions $f_S(\sigma_{sh}(\mathbf{x}), \tau)$ and $f_S(\sigma_1(\mathbf{x}), \tau)$ to inform mechanobiology of chondrocytes [46]. In this work we also included a novel metabolic activity function $f_A(O_2(\mathbf{x}), \tau)$ to inform cellular metabolism based on availability of oxygen.

4.1. Finite element simulations of cartilage during cyclic compression

We exercised our full modeling framework using cyclic, confined compression applied to a
545 full-thickness cartilage explant. Cyclic, confined compression is relevant to walking, running,

and overloading *in-vivo* and presents similar poroelastic creep over time [84, 89], cf. Fig. 2. We choose an axisymmetric representation of our BVP to reduce the computational cost in illustrative simulations, without limiting the generality of our 3-D framework. Simulations required approximately 120 hours on a Linux PC with an Intel Core i7-9700 CPU and 16 GB RAM. Implementing our CMB framework within 3-D FEs facilitates more realistic through-thickness material and structural properties that better reflect the real intra-tissue mechanics of cartilage, similar to our previous work [48, 49, 56, 57].

We observe realistic evolutions of interstitial fluid pressure in our simulations of degeneration similar to early-stage OA. In health, compression of cartilage pressurizes interstitial fluid, as the extracellular matrix has a very low permeability and collagen fibrils direct fluid flow to help prevent fluid exudation [90, 91]. In disease and OA, the previously densely packed proteoglycan and networked collagen are damaged, and thus retarding cartilage’s ability to retain fluid pressure. In Studies 1-3 we observe that fluid pressure decreases slightly as cartilage degenerates (cf. Figs. 3(e), 6(e), and 9(e)) and the porosity increases (cf. Figs. 3(f), 6(f), and 9(f)).

4.2. Studies 1-3: Cartilage degeneration during cyclic overloading

The results from Studies 1 and 2 do not reflect experimental evidence on the evolution of degeneration *in vivo*, i.e. thickness can stabilize [92, 93] and cartilage loss is generally heterogeneous [94, 95]. In Study 1 we considered spatially constant homeostatic values without homeostatic adaptation and spatially constant metabolic activity, i.e. uniform through the thickness. Since there is no adaptation of homeostatic values, cartilage progressively and homogeneously loses thickness under the activation of latent pro-inflammatory cytokines and upregulation of collagenases and aggrecanases (cf. Fig. 4). We included homeostatic adaptation in Study 2 and, as expected, we see cartilage achieves a new equilibrium after approximately 12 months (cf. Fig. 7). Nonetheless, the through-thickness pattern of degeneration remains homogeneous. Experimental evidence suggests that cartilage loss is most pronounced in the SZ and is progressively reduced through the thickness [94], behavior that Studies 1 and 2 fail to capture.

In Study 3 we further included depth-dependent metabolic activity, and results on the evolution of constituents both stabilize and present depth-dependent variations (cf. Fig. 10).

These results are more realistic, as we see greatest degeneration and loss of cell density in the SZ which gradually decreases towards the DZ. Furthermore, the pattern of cartilage degeneration *qualitatively* represents histological images on the progression of OA [95–98]. In Fig. 12 we show full-thickness cross-section of cartilage evolving in Studies 1, 2, and 3 (thus progressively increasing the complexity of our CMB framework) against histological images of progressively degenerated cartilage quantified via the OARSI grading system [96]. Cartilage evolves from healthy (0 month) to progressively degenerated in 12 and 24 months.

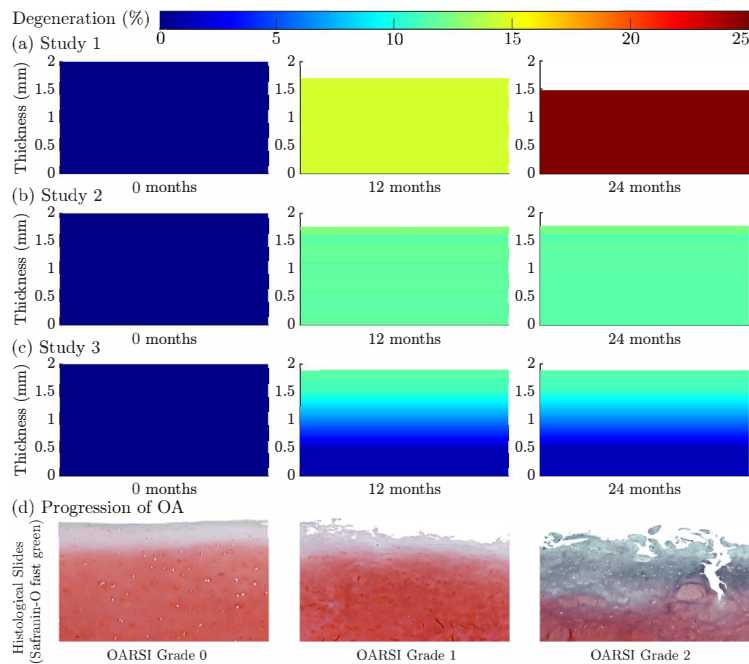


Figure 12: **Full-thickness cross-section of cartilage evolving in Studies 1, 2, and 3 (with progressively increasing complexity of the CMB framework) against histological images of progressively degenerated cartilage (adapted for illustration from Pierce imLab [98]).** Normalized degeneration (i.e. loss of masses of constituents presenting as loss of thickness) at month 0 (baseline), 12, and 24 predicted in (a) Study 1, (b) Study 2, and (c) Study 3. (d) Histological images of progressively degenerated cartilage adapted for illustration from Pierce imLab [98].

In Studies 1 and 2 cartilage homogeneously loses approximately 27% and 11% of its initial thickness, respectively. In study 3, including increased complexity of the CMB framework, cartilage loses approximately 10% of its initial thickness with heterogeneous losses of 12%, 7%, and 2% within the superficial, middle, and deep zones. While no references currently report quantitative data on the through-thickness loss of cartilage thickness it is clear that

the loss is heterogeneous with loss most pronounced within the superficial zone [99].

In our CMB framework, incorporation of oxygen-dependent, and consequently
590 depth-dependent, metabolic activity (exercised in Study 3) yields more realistic numerical
predictions of cartilage degeneration (cf. Fig. 12). This refinement is particularly relevant
as chondrocytes, unlike cells in oxygen-rich tissues such as arteries or muscles, thrive
in hypoxic (low-oxygen) environments. Elevated oxygen levels in cartilage, therefore,
exacerbate degradation processes more than hypoxic conditions [100, 101]. Furthermore,
595 there is compelling evidence linking oxidative stress to progressive cartilage degeneration
[102, 103]. Recent advancements in strategies to treat OA focused on mitigating oxidative
damage by reducing the production of nitric oxide and reactive oxygen species through
hypoxia-based interventions [104]. The discovery of hypoxia-inducible factor has further
invigorated this research direction, with experimental findings suggesting that hypoxia not
600 only inhibits cartilage degradation but also promotes its regeneration [105].

4.3. Limitations and outlook

To establish and exercise our chemo-mechano-biological framework we focus on a select
group of “minimally essential” signaling pathways while recognizing many more exist [106].
We categorize chemical species based on their general roles in the evolution of cartilage
605 although there are variations in specific impacts within these categories. Specific proportions
of these chemical species within cartilage remain unknown. Our model assumes chondrocytes
alone produce cytokines and enzymes. However, fibroblasts, macrophages, and synoviocytes
outside cartilage also express pro-inflammatory cytokines, collagenases, and aggrecanases
that contribute to cartilage degradation [107, 108]. Latent growth factors, for example, can
610 also be activated by reactive oxygen species (ROS), nitric oxide (NO), MMP3, and protein
interactions, in addition to shear stresses [72, 73]. While incorporation of depth-dependent
metabolic activity (exercised in Study 3) yields more realistic numerical predictions of
cartilage degeneration we acknowledge that a (relatively simple) depth-dependent tuning
parameter may not fully capture realistic heterogeneity. With more experimental data, we
615 can better calibrate and validate our framework, thus refining model parameters, or even
extend the complexity of our framework. Our framework could be extended using additional
ODEs, for example, to model time-dependent hypoxia-inducible factor-1 α (HIF-1 α) signaling

that stabilizes the cartilage phenotype [109] and sustains chondrocyte metabolism [109–111].

We implemented our framework within 3-D nonlinear FEs, an advancement that affords
620 much greater versatility, specifically in representing intra-cartilage heterogeneity and by
enabling diverse BVPs. We included our image-driven, heterogeneous constitutive model
of cartilage [48], as well as the mechanical effects of osmotic swelling [49], to capture
through-thickness heterogeneity in intra-cartilage mechanics. We proposed metabolic
cell activity driven by the local availability of oxygen, an advancement that introduces
625 realistic, through-thickness patterns of degeneration in cartilage. To enable patient-specific
analyses within our framework we have also established a fully automated and publicly
available workflow to generate patient-specific models from research or clinical Magnetic
Resonance Images (MRIs). First, we provide a customized convolutional neural network to
automatically segment MRIs of human knees [112]. Second, we provide custom software to
630 then automatically generate hexahedral meshes of patient-specific structures of the human
knee, i.e. femoral/tibial cartilages and menisci, faithfully representing the geometries with
high-quality FEs [113]. Our novel suite of software tools will allow us and others to advance
understanding of patient-specific pathological changes due to biomechanical factors, improve
clinical diagnostics and therapies, and enable new methods for non-invasive diagnosis and
635 pre-/post-operative decision making. Our chemo-mechano-biological framework for evolving
cartilage is publicly available for download and academic use as a plugin for FEBio at
<https://github.uconn.edu/imLab/FEVGnR-Plugin>.

Acknowledgments

We thank Steve Maas for his thoughtful assistance with FEBio.

640 Ethical Approval

We do not need ethical approval.

Funding

National Science Foundation (NSF) award 1662429 and Royal Society International
Exchange award (IES\R3\233163).

We declare no competing interests.

Appendix A

In Fig. 13 we show direct comparison of our original implementation within MATLAB R2021b (including a hyperelastic constitutive model of cartilage) [46] with our implementation using FEBio 4.2 (including a biphasic constitutive model of cartilage). Our

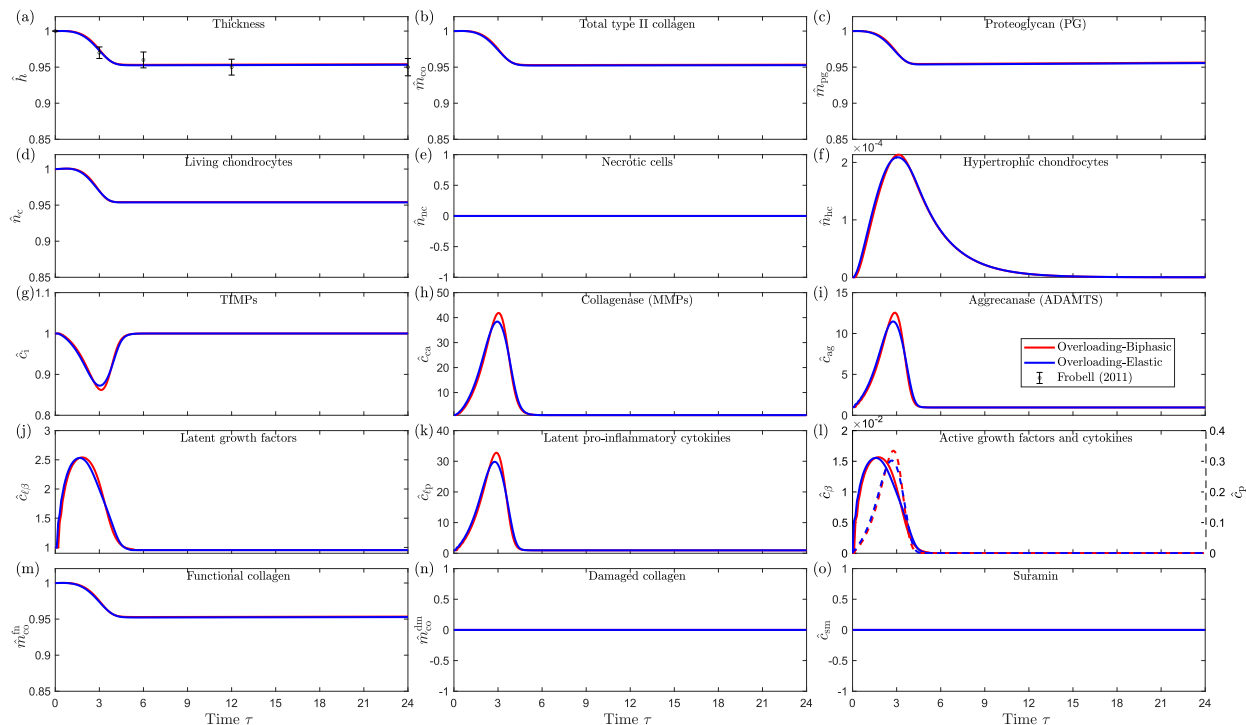


Figure 13: **Direct comparison of the evolution of cartilage during overloading simulated within MATLAB R2021b (hyperelastic) [46] and within FEBio 4.2 (biphasic).**

650

simulation using FEBio leverages a single, unit-cube finite element to verify the correct implementation of our system of ODEs (12) - (24).

Appendix B

In Tables 6 and 7 we list the model parameters for our signaling-pathways biochemical

655 model of cartilage (§2.2) [46].

Table 6: **Cellular and structural rate parameters for cartilage [46].** Definitions, values, and references.

Parameter	Definition	Value [month ⁻¹]	Notes and References
r_1^c	Rate of baseline chondrocytes proliferation	4.5×10^{-2}	Equal r_3^c ; balancing source/sink terms at homeostasis
r_2^c	Rate of chondrocytes population dynamics sensitivity to anabolic cytokines and growth factors	4.0×10^{-1}	Combined anabolic cytokines and growth factor effects [69] [114]
r_3^c	Rate of baseline chondrocytes death	4.5×10^{-2}	Extrapolating the apoptosis rate of normal chondrocytes [115]
r_4^c	Rate of proliferating chondrocytes converting into hypertrophic chondrocytes	1.0×10^{-2}	Growth factors cause proliferation; fraction of the proliferating chondrocytes become hypertrophic [69] [116]
r_5^c	Rate of activated pro-inflammatory cytokines driven cell death	1.0×10^{-1}	Pro-inflammatory cytokines cause cell death [60]
r_1^{hc}	Rate of proliferating chondrocytes converting into hypertrophic chondrocytes	1.0×10^{-2}	Equal to r_4^c , cellular species conversion; Growth factors cause proliferation; fraction of the proliferating chondrocytes become hypertrophic
r_2^{hc}	Rate of baseline hypertrophic chondrocytes death	4.5×10^{-1}	
r_1^{nc}	Rate of baseline necrotic chondrocytes death	1.0×10^0	Fraction of normal chondrocytes become necrotic due to high impact injurious loading
r_1^{co}	Rate of baseline collagen deposition by chondrocytes	6.4×10^{-4}	Equal r_3^{co} ; balancing source/sink terms at homeostasis
r_2^{co}	Rate of growth factors driven increase in collagen deposition by chondrocytes	1.0×10^{-1}	Growth factors increase collagen deposition [117]
r_3^{co}	Rate of collagenase-driven functional collagen degradation	6.4×10^{-4}	Based on the half lives of collagen in cartilage [118]
r_4^{co}	Rate of collagenase-driven damaged collagen degradation	1.0×10^0	Damaged collagen degrades faster than functional collagen
r_1^{pg}	Rate of baseline proteoglycan deposition by chondrocytes	2.3×10^{-3}	Equal r_3^{pg} ; balancing source/sink terms at homeostasis
r_2^{pg}	Rate of growth factors driven increase in proteoglycan deposition by chondrocytes	1.0×10^{-1}	Growth factors increase PG deposition [117]
r_3^{pg}	Rate of aggrecanase-driven proteoglycan degradation	2.3×10^{-3}	Based on the half lives of PG in cartilage [119, 120]

Table 7: **Biochemical rate parameters for cartilage [46]**. Definitions, values, and references.

Parameter	Definition	Value [month ⁻¹]	Notes and References
$r_1^{\ell\beta}$	Rate of baseline latent growth factors secretion by chondrocytes	5.0×10^1	Equal $r_3^{\ell\beta}$; balancing source/sink
$r_2^{\ell\beta}$	Rate of latent growth factor secretion by chondrocytes mediated by active growth factors	5.0×10^3	
$r_3^{\ell\beta}$	Rate of baseline degradation of latent growth factors	5.0×10^1	Based on half lives of growth factors in cartilage [121–123]
$r_4^{\ell\beta}$	Rate of latent growth factor converting to active form by mechanical stimuli	5.0×10^{-1}	Active growth factor has very low concentration in cartilage [124]
r_1^β	Rate of latent growth factor converting to active form by mechanical stimuli	5.0×10^{-1}	Equal to $r_4^{\ell\beta}$, cellular species conversion
r_2^β	Rate of baseline degradation of active growth factor	5.0×10^1	Equal $r_3^{\ell\beta}$; same rate of degradation as latent growth factors
$r_1^{\ell p}$	Rate of baseline latent pro-inflammatory cytokines secretion by chondrocytes	5.0×10^1	Equal $r_5^{\ell p}$; balancing source/sink
$r_2^{\ell p}$	Rate of latent pro-inflammatory cytokines secretion by chondrocytes triggered by active cytokines	5.0×10^3	
$r_3^{\ell p}$	Rate of latent pro-inflammatory cytokines inhibition by active growth factors	1.0×10^0	
$r_4^{\ell p}$	Rate of baseline latent pro-inflammatory cytokines secretion by necrotic chondrocytes	5.0×10^0	
$r_5^{\ell p}$	Rate of baseline degradation of latent pro-inflammatory cytokines	5.0×10^1	Based on half lives of pro-inflammatory cytokines in cartilage [125–127]
$r_6^{\ell p}$	Rate of latent pro-inflammatory cytokines converting to active form by mechanical stimuli	1.0×10^0	Active pro-inflammatory cytokines has very low concentration in cartilage
r_1^p	Rate of latent pro-inflammatory cytokines converting to active form by mechanical stimuli	5.0×10^{-1}	Equal to $r_6^{\ell p}$, cellular species conversion
r_2^p	Rate of baseline degradation of active pro-inflammatory cytokines	5.0×10^1	Equal $r_5^{\ell p}$; same rate of degradation as latent pro-inflammatory cytokines

Table 7: **Biochemical rate parameters.** Definitions, values, and references (cont. I).

Parameter	Definition	Value [month ⁻¹]	Notes and References
r_1^{ca}	Rate of baseline collagenase secretion by chondrocytes	4.6×10^0	Equal $r_5^{ca} + r_6^{ca}$; balancing source/sink terms at homeostasis
r_2^{ca}	Rate of pro-inflammatory cytokines-driven upregulation in collagenase secretion by chondrocytes	6.0×10^2	
r_3^{ca}	Rate of growth factors-driven downregulation in collagenase secretion by chondrocytes	1.0×10^0	
r_4^{ca}	Rate of baseline collagenase secretion by hypertrophic chondrocytes	1.0×10^2	Hypertrophic chondrocytes express collagenases [128]
r_5^{ca}	Rate of baseline collagenase degradation	4.2×10^0	Based on the half lives of collagenase in cartilage [42, 129]
r_6^{ca}	Rate of TIMP-mediated collagenase degradation	$0.1r_4^{ca} = 4.2 \times 10^{-1}$	Assuming additional 10% degradation by TIMP complex of collagenase and aggrecanase [42]
r_1^{ag}	Rate of baseline aggrecanase secretion by chondrocytes	1.4×10^2	Equal $r_5^{ag} + r_6^{ag}$; balancing source/sink terms at homeostasis
r_2^{ag}	Rate of pro-inflammatory cytokines-driven upregulation in aggrecanase secretion by chondrocytes	5.0×10^3	
r_3^{ag}	Rate of growth factors-driven downregulation in aggrecanase secretion by chondrocytes	1.0×10^0	
r_4^{ag}	Rate of baseline aggrecanase secretion by hypertrophic chondrocytes	1.0×10^2	Hypertrophic chondrocytes express aggrecanases [128]
r_5^{ag}	Rate of baseline aggrecanase degradation	1.4×10^2	Based on the half lives of aggrecanase in cartilage [130]
r_6^{ag}	Rate of TIMP-mediated aggrecanase degradation	4.2×10^{-1}	Equal to r_6^{ca} ; additional degradation by TIMP complex of collagenase and aggrecanase [42]

Table 7: **Biochemical rate parameters.** Definitions, values, and references (cont. II).

Parameter	Definition	Value [month ⁻¹]	Notes and References
r_1^i	Rate of baseline TIMP secretion by chondrocytes	1.4×10^2	Equal $r_3^i + r_4^i + r_5^i$; balancing source/sink
r_2^i	Rate of growth factors-driven increase in TIMP by chondrocytes	1.0×10^{-1}	
r_3^i	Rate of baseline TIMP degradation and uptake by chondrocytes	1.4×10^2	Based on the half lives of aggrecanase in cartilage [131]
r_4^i	Rate of TIMP degradation of TIMP and collagenase complex	4.2×10^{-1}	Equal r_6^{ca}
r_5^i	Rate of TIMP degradation of TIMP and aggrecanase complex	4.2×10^{-1}	Equal r_6^{ag}

References

- [1] R. F. Loeser, S. R. Goldring, C. R. Scanzello, M. B. Goldring, Osteoarthritis: A disease of the joint as an organ, *Arthritis Rheum.* 64 (2012) 1697–1707.
- [2] R. C. Lawrence, D. T. Felson, C. G. Helmick, L. M. Arnold, H. Choi, R. A. Deyo, S. Gabriel, R. Hirsch, M. C. Hochberg, G. G. Hunder, J. M. Jordan, J. N. Katz, H. M. Kremers, F. Wolfe, Estimates of the prevalence of arthritis and other rheumatic conditions in the United States: Part II, *Arthritis Rheum.* 58 (2008) 26–35.
- [3] V. C. Mow, R. Huiskes, Structure and function of ligaments and tendons, in: S. L.-Y. Woo, T. Q. Lee, S. D. Abramowitch, T. W. Gilbert (Eds.), *Basic Orthopaedic Biomechanics and Mechano-Biology*, 3rd Edition, Lippincott Williams & Wilkins, Philadelphia, 2005, pp. 301–342.
- [4] N. D. Broom, D. L. Marra, Ultrastructural evidence for fibril-to-fibril associations in articular cartilage and their functional implication, *J. Anat.* 146 (1986) 185–200.
- [5] W. B. Zhu, V. C. Mow, T. J. Koob, D. R. Eyre, Viscoelastic shear properties of articular cartilage and the effects of glycosidase treatments, *J. Orthop. Res.* 11 (1993) 771–781.
- [6] C. Chen, D. T. Tambe, L. Deng, L. Yang, Biomechanical properties and

mechanobiology of the articular chondrocyte, *Am. J. Physiol., Cell Physiol.* 305 (2013) C1202–C1208.

- 675 [7] S. D. Waldman, C. G. Spiteri, M. D. Gryn timer, R. M. Pilliar, J. Hong, R. A. Kandel, Effect of biomechanical conditioning on cartilaginous tissue formation in vitro, *J. Bone Joint Surg.* 85 (2003) 101–105.
- [8] M. Wong, M. Siegrist, K. Goodwin, Cyclic tensile strain and cyclic hydrostatic pressure differentially regulate expression of hypertrophic markers in primary chondrocytes, 680 *Bone* 33 (2003) 685–693.
- [9] J. A. Buckwalter, H. J. Mankin, A. J. Grodzinsky, Articular cartilage and osteoarthritis, in: V. D. Pellegrini (Ed.), *AAOS Instructional Course Lectures*, Vol. 54, American Academy of Orthopaedic Surgeons, Rosemont, IL, 2005, pp. 465–480.
- [10] J. P. G. Urban, The chondrocyte: a cell under pressure, *Rheumatology* 33 (1994) 685 901–908.
- [11] R. L. Smith, J. Lin, M. C. D. Trindade, J. Shida, G. Kajiyama, T. Vu, A. R. Hoffman, M. C. H. van der Meulen, S. B. Goodman, D. J. Schurman, D. R. Carter, Time-dependent effects of intermittent hydrostatic pressure on articular chondrocyte type ii collagen and aggrecan mRNA expression, *J. Radiat. Res. Dev.* 37 (2000).
- 690 [12] K. Honda, S. Ohno, K. Tanimoto, C. Ijuin, N. Tanaka, T. Doi, Y. Kato, K. Tanne, The effects of high magnitude cyclic tensile load on cartilage matrix metabolism in cultured chondrocytes, *Eur. J. Cell Biol.* 79 (2000) 601–609.
- [13] M. B. Goldring, K. B. Marcu, Cartilage homeostasis in health and rheumatic diseases, *Arthritis Res. Ther.* 11 (2009) 224, pMC2714092.
- 695 [14] M. Anghelina, D. Sjostrom, P. Perera, J. Nam, T. Knobloch, S. Agarwal, Regulation of biomechanical signals by NF- κ B transcription factors in chondrocytes, *Biorheology* 45 (2008) 245–256.
- [15] K. B. Marcu, M. Otero, E. Olivetto, R. M. Borzi, M. B. Goldring, NF- κ B Signaling: Multiple Angles to Target OA, *Curr. Drug Targets* 11 (2010) 599–613.

- 700 [16] D. L. Bader, D. M. Salter, T. T. Chowdhury, Biomechanical influence of cartilage homeostasis in health and disease, *Arthritis* (2011) 979032, 16PMC3196252.
- [17] E. Y. Salinas, J. C. Hu, K. Athanasiou, A Guide for Using Mechanical Stimulation to Enhance Tissue-Engineered Articular Cartilage Properties, *Tissue Eng. Part B Rev.* 24 (2018) 345–358.
- 705 [18] C. J. Hunter, S. M. Imler, P. Malaviya, R. M. Nerem, M. E. Levenston, Mechanical compression alters gene expression and extracellular matrix synthesis by chondrocytes cultured in collagen i gels, *Biomat.* 23 (2002) 1249–1259.
- [19] Z. Peng, H. Sun, V. Bunpetch, Y. Koh, Y. Wen, D. Wu, H. Ouyang, The regulation of cartilage extracellular matrix homeostasis in joint cartilage degeneration and
710 regeneration, *Biomaterials* 268 (2021) 120555.
- [20] L. C. Tetlow, D. J. Adlam, D. E. Woolley, Matrix metalloproteinase and proinflammatory cytokine production by chondrocytes of human osteoarthritic cartilage: Associations with degenerative changes, *Arthritis Rheum.* 44 (2001) 585–594.
- [21] E. Charlier, B. Relic, C. Deroyer, O. Malaise, S. Neuville, J. Collée, M. Malaise, D. De
715 Seny, Insights on Molecular Mechanisms of Chondrocytes Death in Osteoarthritis, *Int. J. Mol. Sci.* 17 (2016) 2146.
- [22] L. J. Sandell, T. Aigner, Articular cartilage and changes in arthritis. an introduction: Cell biology of osteoarthritis, *Arthritis Res.* 3 (2001) 107–113.
- [23] M. B. Goldring, The role of the chondrocyte in osteoarthritis, *Arthritis Rheum.* 43
720 (2000) 1916–1926.
- [24] T. Aigner, B. Kurz, N. Fukui, L. Sandell, Roles of chondrocytes in the pathogenesis of osteoarthritis, *Curr. Opin. Rheumatol.* 14 (2002) 578–584.
- [25] T. Tallheden, C. Bengtsson, C. Brantsing, E. Sjögren-Jansson, L. Carlsson, L. Peterson, M. Brittberg, A. Lindahl, Proliferation and differentiation potential of chondrocytes
725 from osteoarthritic patients, *Arthritis Res. Ther.* 7 (2005) R560–R568.

- [26] K. P. H. Pritzker, S. Gay, S. A. Jimenez, K. Ostergaard, J. P. Pelletier, P. A. Revell, D. Salter, W. B. van den Berg, Osteoarthritis cartilage histopathology: grading and staging, *Osteoarthritis and Cartilage* 14 (2006) 13–29.
- [27] T. Aigner, S. Söder, P. M. Gebhard, A. McAlinden, J. Haag, Mechanisms of disease: role of chondrocytes in the pathogenesis of osteoarthritis-structure, chaos and senescence, *Nat. Rev. Rheumatol.* 3 (2007) 391–399.
- [28] P. Wojdasiewicz, L. A. Poniatowski, D. Szukiewicz, The role of inflammatory and anti-inflammatory cytokines in the pathogenesis of osteoarthritis, *Mediators of Inflammation* 2014 (2014) 561459.
- [29] K. Yamamoto, D. Wilkinson, G. Bou-Gharios, Targeting Dysregulation of Metalloproteinase Activity in Osteoarthritis, *Calcif. Tissue Int.* 109 (2021) 277–290.
- [30] X. Houard, M. B. Goldring, F. Berenbaum, Homeostatic mechanisms in articular cartilage and role of inflammation in osteoarthritis, *Curr. Rheumatol. Rep.* 15 (2013) 375.
- [31] S. Ströbel, M. Loparic, D. Wendt, A. D. Schenk, C. Candrian, R. L. Lindberg, F. Moldovan, A. Barbero, I. Martin, Anabolic and catabolic responses of human articular chondrocytes to varying oxygen percentages, *Arthritis Res. Ther.* 12 (2010) R34.
- [32] L.-Y. Chen, M. Lotz, R. Terkeltaub, R. Liu-Bryan, Modulation of matrix metabolism by ATP-citrate lyase in articular chondrocytes, *J. Bio. Chem.* 293 (2018) 12259–12270.
- [33] L. Jain, S. M. Bolam, A. P. Monk, J. T. Munro, E. Chen, J. Tamatea, N. Dalbeth, R. C. Poulsen, Differential effects of hypoxia versus hyperoxia or physoxia on phenotype and energy metabolism in human chondrocytes from osteoarthritic compared to macroscopically normal cartilage, *Int. J. Mol. Sci.* 24 (2023).
- [34] A. Davol, M. S. Bingham, R. L. Sah, S. M. Klisch, A nonlinear finite element model of cartilage growth, *Biomech. Model. Mechanobiol.* 7 (2008) 295–307.

- [35] N. S. Landinez-Parra, D. A. Garzón-Alvarado, J. C. Vanegas-Acosta, A phenomenological mathematical model of the articular cartilage damage, *Comput. Methods Programs Biomed.* 104 (2011) e58–e74.
- 755 [36] S. M. Hosseini, W. Wilson, K. Ito, C. C. Van Donkelaar, A numerical model to study mechanically induced initiation and progression of damage in articular cartilage, *Osteoarthritis and Cartilage* 22 (2014) 95–103.
- [37] C. Bandejas, A. Completo, A mathematical model of tissue-engineered cartilage development under cyclic compressive loading, *Biomech. Model. Mechanobiol.* 16
760 (2017) 651–666.
- [38] M. K. Liukkonen, M. E. Mononen, O. Klets, J. P. Arokoski, S. Saarakkala, R. K. Korhonen, Simulation of subject-specific progression of knee osteoarthritis and comparison to experimental follow-up data: Data from the osteoarthritis initiative, *Sci. Rep.* 7 (2017) 1–14.
- 765 [39] G. A. Orozco, P. Tanska, C. Florea, A. J. Grodzinsky, R. K. Korhonen, A novel mechanobiological model can predict how physiologically relevant dynamic loading causes proteoglycan loss in mechanically injured articular cartilage, *Sci. Rep.* 8 (2018) 15599.
- [40] M. E. Mononen, M. K. Liukkonen, R. K. Korhonen, Utilizing Atlas-Based Modeling
770 to Predict Knee Joint Cartilage Degeneration: Data from the Osteoarthritis Initiative, *Ann. Biomed. Eng.* 47 (2019) 813–825.
- [41] M. Baker, B. S. Brook, M. R. Owen, Mathematical modelling of cytokines, MMPs and fibronectin fragments in osteoarthritic cartilage, *J. Math. Biol.* 75 (2017) 985–1024.
- [42] N. Moise, A. Friedman, Rheumatoid arthritis - a mathematical model, *J. Theor. Biol.*
775 461 (2019) 17–33.
- [43] G. I. Kapitanov, X. Wang, B. P. Ayati, M. J. Brouillette, J. A. Martin, Linking cellular and mechanical processes in articular cartilage lesion formation: A mathematical model, *Frontiers in Bioengineering and Biotechnology* 4 (2016).

- [44] A. S. Eskelinen, P. Tanska, C. Florea, G. A. Orozco, P. Julkunen, A. J. Grodzinsky, R. K. Korhonen, Mechanobiological model for simulation of injured cartilage degradation via proinflammatory cytokines and mechanical, *PLoS Comput. Biol.* 16 (2020) 1–25.
- [45] M. Segarra-Queralt, G. Piella, J. Noailly, Network-based modelling of mechano-inflammatory chondrocyte regulation in early osteoarthritis, *Front. Bioeng. Biotechnol.* 11 (2023) 1–17.
- [46] M. M. Rahman, P. N. Watton, C. P. Neu, D. M. Pierce, A chemo-mechano-biological modeling framework for cartilage evolving in health, disease, injury, and treatment, *Comput. Methods Programs Biomed.* 231 (2023) 107419.
- [47] J. Sanchez-Adams, H. A. Leddy, A. L. McNulty, C. J. O’Conor, F. Guilak, The Mechanobiology of Articular Cartilage: Bearing the Burden of Osteoarthritis, *Curr. Rheumatol. Rep.* 16 (2014) 1–9.
- [48] D. M. Pierce, M. J. Unterberger, W. Trobin, T. Ricken, G. A. Holzapfel, A microstructurally based continuum model of cartilage viscoelasticity and permeability incorporating statistical fiber orientation, *Biomech. Model. Mechanobiol.* 15 (2016) 229–244.
- [49] X. Wang, T. S. E. Eriksson, T. Ricken, D. M. Pierce, On incorporating osmotic prestretch/prestress in image-driven finite element simulations of cartilage, *J. Mech. Behav. Biomed. Mat.* 86 (2018) 409–422.
- [50] A. Grytsan, T. S. E. Eriksson, P. N. Watton, T. C. Gasser, Growth description for VesselWall adaptation: A Thick-Walled mixture model of abdominal aortic aneurysm evolution, *Materials* 10 (2017) 1–19.
- [51] R. De Boer, *Theory of porous media: highlights in historical development and current state*, Springer-Verlag, Heidelberg, 2000.
- [52] T. J. Pence, On the formulation of boundary value problems with the incompressible

- 805 constituents constraint in finite deformation poroelasticity, *Math. Method Appl. Sci.* 35 (2012) 1756–1783.
- [53] N. Karajan, An extended biphasic description of the inhomogeneous and anisotropic intervertebral disc, Ph.D. thesis, Universität Stuttgart, Holzgartenstr. 16, 70174 Stuttgart (2009).
- 810 [54] J. C. Chen, K. S. Pister, Remarks on rate constitutive equations for finite deformation problems: computational implications, *Comput. Meth. Appl. Mech. Eng.* 46 (1984) 201–215.
- [55] J. Bluhm, Modelling of saturated thermo-elastic porous solids with different phase temperatures. In: Ehlers W, Bluhm J (eds) *Porous media: theory, experiments and numerical applications*, Springer-Verlag, Berlin, Heidelberg, New York, 2002.
- 815 [56] D. M. Pierce, T. Ricken, G. A. Holzapfel, A hyperelastic biphasic fiber-reinforced model of articular cartilage considering distributed collagen fiber orientations: Continuum basis, computational aspects and applications, *Comput. Methods Biomech. Biomed. Engin.* 16 (2013) 1344–1361.
- 820 [57] D. M. Pierce, T. Ricken, G. A. Holzapfel, Modeling sample/patient-specific structural and diffusional response of cartilage using DT-MRI, *Int. J. Numer. Meth. Biomed. Engng.* 29 (2013) 807–821.
- [58] G. Eipper, Theorie und numerik finiter elastischer deformationen in fluidgesättigten porösen Festkörpern, Ph.D. Dissertation, Universität Stuttgart (1998).
- 825 [59] T. Tallheden, C. Bengtsson, C. Brantsing, E. Sjögren-Jansson, L. Carlsson, L. Peterson, M. Brittberg, A. Lindahl, Proliferation and differentiation potential of chondrocytes from osteoarthritic patients, *Arthritis Res. Ther.* 7 (2005).
- [60] A. J. Schuerwegh, E. J. Dombrecht, W. J. Stevens, J. F. Van Offel, C. H. Bridts, L. S. De Clerck, Influence of pro-inflammatory (IL-1 α , IL-6, TNF- α , IFN- γ) and anti-inflammatory (IL-4) cytokines on chondrocyte function, *Osteoarthritis and Cartilage* 11 (2003) 681–687.
- 830

- [61] W. Madej, A. van Caam, E. N. Blaney Davidson, P. M. van der Kraan, P. Buma, Physiological and excessive mechanical compression of articular cartilage activates Smad2/3P signaling, *Osteoarthritis and Cartilage* 22 (2014) 1018–1025.
- 835 [62] P. F. Argote, J. T. Kaplan, A. Poon, X. Xu, L. Cai, N. C. Emery, D. M. Pierce, C. P. Neu, Chondrocyte viability is lost during high-rate impact loading by transfer of amplified strain, but not stress, to pericellular and cellular regions, *Osteoarthritis and Cartilage* 27 (2019) 1822–1830.
- [63] A. J. Sophia Fox, A. Bedi, S. A. Rodeo, The basic science of articular cartilage: Structure, composition, and function, *Sports Health* 1 (2009) 461–468.
- 840 [64] L. A. Fortier, J. U. Barker, E. J. Strauss, T. M. McCarrel, B. J. Cole, The role of growth factors in cartilage repair, *Clin. Orthop. Relat. Res.* 469 (2011) 2706–2715.
- [65] E.-S. E. Mehana, A. F. Khafaga, S. S. El-Blehi, The role of matrix metalloproteinases in osteoarthritis pathogenesis: An updated review, *Life Sci.* 234 (2019) 116786.
- 845 [66] P. Verma, K. Dalal, ADAMTS-4 and ADAMTS-5: Key enzymes in osteoarthritis, *J. Cell Biochem.* 112 (2011) 3507–3514.
- [67] M. B. Goldring, M. Otero, D. A. Plumb, C. Dragomir, M. Favero, K. El Hachem, K. Hashimoto, H. I. Roach, E. Olivotto, R. M. Borzi, K. B. Marcu, Roles of inflammatory and anabolic cytokines in cartilage metabolism: signals and multiple effectors converge upon MMP-13 regulation in osteoarthritis, *Eur. Cell Mater.* 21
- 850 (2011) 202–220.
- [68] A. E. M. Jørgensen, M. Kjær, K. M. Heinemeier, The Effect of Aging and Mechanical Loading on the Metabolism of Articular Cartilage, *J. Rheumatol.* 44 (2017) 410–417.
- [69] N. G. M. Thielen, P. M. van der Kraan, A. P. M. van Caam, TGF β /bmp signaling pathway in cartilage homeostasis, *Cells* 8 (2019) 969.
- 855 [70] P. M. Van der Kraan, W. B. Van den Berg, Chondrocyte hypertrophy and osteoarthritis: Role in initiation and progression of cartilage degeneration?, *Osteoarthritis and Cartilage* 20 (2012) 223–232.

- [71] C. P. Neu, A. Khalafi, K. Komvopoulos, T. M. Schmid, A. H. Reddi, 860
Mechanotransduction of bovine articular cartilage superficial zone protein by
transforming growth factor β signaling, *Arthritis Rheum.* 56 (2007) 3706–3714.
- [72] M. B. Albro, A. D. Cigan, R. J. Nims, K. J. Yeroushalmi, S. R. Oungoulian, C. T.
Hung, G. A. Ateshian, Shearing of synovial fluid activates latent TGF- β , *Osteoarthritis
and Cartilage* 20 (2012) 1374–1382.
- 865 [73] M. B. Albro, R. J. Nims, A. D. Cigan, K. J. Yeroushalmi, T. Alliston, C. T. Hung,
G. A. Ateshian, Accumulation of exogenous activated TGF- β in the superficial zone
of articular cartilage, *Biophys. J.* 104 (2013) 1794–1804.
- [74] P. Limraksasin, Y. Kosaka, M. Zhang, N. Horie, T. Kondo, H. Okawa, M. Yamada,
H. Egusa, Shaking culture enhances chondrogenic differentiation of mouse induced
870 pluripotent stem cell constructs, *Sci. Rep.* 10 (2020) 14996.
- [75] M. Yanoshita, N. Hirose, Y. Okamoto, C. Sumi, M. Takano, S. Nishiyama,
Y. Asakawa-Tanne, K. Horie, A. Onishi, Y. Yamauchi, T. Mitsuyoshi, R. Kunimatsu,
K. Tanimoto, Cyclic tensile strain upregulates pro-inflammatory cytokine expression
via fak-mapk signaling in chondrocytes, *Inflammation* 41 (2018) 1621–1630.
- 875 [76] Y. Sun, P. Leng, M. Song, D. Li, P. Guo, X. Xu, H. Gao, Z. Li, C. Li, H. Zhang, Piezo1
activates the nlrp3 inflammasome in nucleus pulposus cell-mediated by $ca^{2+}/nf-\kappa b$
pathway, *Int. Immunopharmacol.* 85 (2020) 106681.
- [77] Z. Sun, X. Zheng, S. Li, J. Zeng, Baozhuand Yang, Z. Ling, X. Liu, F. Wei,
Single impact injury of vertebral endplates without structural disruption, initiates
880 disc degeneration through piezo1 mediated inflammation and metabolism dysfunction,
Spine 47 (2022) E203–E213.
- [78] W. C. Aird, Spatial and temporal dynamics of the endothelium, *J. Thromb. Haemost.*
3 (2005) 1392–1406.
- 885 [79] P. Aparício, A. Mandaltsi, J. Boamah, H. Chen, A. Selimovic, M. Bratby, R. Uberoi,
Y. Ventikos, P. Watton, Modelling the influence of endothelial heterogeneity on the

progression of arterial disease: application to abdominal aortic aneurysm evolution, *Int. J. Numer. Meth. Biomed. Eng.* 30 (2014) 563–586.

[80] S. A. Maas, B. J. Ellis, G. A. Ateshian, J. A. Weiss, FEBio: Finite Elements for Biomechanics, *J. Biomech. Eng.* 134 (2012) 011005.

890 [81] J. T. Kaplan, C. P. Neu, H. Drissi, N. C. Emery, D. M. Pierce, Cyclic loading of human articular cartilage: The transition from compaction to fatigue, *J. Mech. Behav. Biomed. Mat.* 65 (2017) 734–742.

[82] M. S. Kuster, G. A. Wood, G. W. Stachowiak, A. Gächter, Joint load considerations in total knee replacement, *J. Bone Joint Surg.* 79 (1997) 109–113.

895 [83] S. C. Walpole, D. Prieto-Merino, P. Edwards, J. Cleland, G. Stevens, I. Roberts, The weight of nations: an estimation of adult human biomass, *BMC Public Health* 12 (2012) 1–6.

[84] C. S. Paranjape, H. C. Cutcliffe, S. C. Grambow, G. M. Utturkar, A. T. Collins, W. E. Garrett, C. E. Spritzer, L. E. DeFrate, A New Stress Test for Knee Joint Cartilage, *Sci. Rep.* 9 (2019) 1–8.

900

[85] S. Grenier, M. M. Bhargava, P. A. Torzilli, An in vitro model for the pathological degradation of articular cartilage in osteoarthritis, *J. Biomech.* 47 (2014) 645–652.

[86] J. A. Wahlquist, F. W. DelRio, M. A. Randolph, A. H. Aziz, C. M. Heveran, S. J. Bryant, C. P. Neu, V. L. Ferguson, Indentation mapping revealed poroelastic, but not viscoelastic, properties spanning native zonal articular cartilage, *Acta Biomater.* 64 (2017) 41–49.

905

[87] J. D. Humphrey, M. A. Schwartz, Vascular mechanobiology: Homeostasis, adaptation, and disease, *Annu. Rev. Biomed. Eng.* 23 (Volume 23, 2021) (2021) 1–27.

[88] Q. A. Meslier, S. J. Shefelbine, Using Finite Element Modeling in Bone Mechanoadaptation, *Curr. Osteoporos. Rep.* 21 (2) (2023) 105–116.

910

- [89] C. G. Armstrong, V. C. Mow, Variations in the intrinsic mechanical properties of human articular cartilage with age, degeneration, and water content, *J. Bone Joint Surg. Am.* 64 (1982) 88–94.
- [90] P. A. Torzilli, D. A. Dethmers, D. E. Rose, H. F. Schryuer, Movement of interstitial water through loaded articular cartilage, *J. Biomech.* 16 (3) (1983) 169–179.
- [91] H. Guo, S. A. Maher, P. A. Torzilli, A biphasic finite element study on the role of the articular cartilage superficial zone in confined compression, *J. Biomech.* 48 (2015) 166–170.
- [92] Vanwanseele, F. Eckstein, H. Knecht, E. Stüssi, A. Spaepen, Knee cartilage of spinal cord-injured patients displays progressive thinning in the absence of normal joint loading and movement, *Arthritis Rheum.* 46 (2002) 2073–2078.
- [93] R. B. Frobell, Change in cartilage thickness, posttraumatic bone marrow lesions, and joint fluid volumes after acute ACL disruption: A two-year prospective MRI study of sixty-one subjects, *J. Bone Joint Surg.* 93 (2011) 1096–1103.
- [94] A. R. Poole, An introduction to the pathophysiology of osteoarthritis, *Front. Biosci.* 4 (4) (1999) 662–670.
- [95] W. Waldstein, G. Perino, S. L. Gilbert, S. A. Maher, R. Windhager, F. Boettner, Oarsi osteoarthritis cartilage histopathology assessment system: A biomechanical evaluation in the human knee, *J. Orthop. Res.* 34 (2016) 135–140.
- [96] K. P. H. Pritzker, S. Gay, S. A. Jimenez, K. Ostergaard, J.-P. Pelletier, P. A. Revell, D. Salter, W. B. van den Berg, Osteoarthritis cartilage histopathology: grading and staging, *Osteoarthritis and Cartilage* 14 (2006) 13–29.
- [97] C. Pauli, R. Whiteside, F. L. Heras, D. Nesic, J. Koziol, S. P. Grogan, J. Matyas, K. P. H. Pritzker, D. D. D’Lima, M. K. Lotz, Comparison of cartilage histopathology assessment systems on human knee joints at all stages of osteoarthritis development, *Osteoarthritis and Cartilage* 20 (2012) 476–485.

- [98] F. Maier, C. G. Lewis, D. M. Pierce, The evolving large-strain shear responses of progressively osteoarthritic human cartilage, *Osteoarthritis and Cartilage* 27 (2019) 810–822.
- 940 [99] B. Rolauffs, C. Muehleman, J. Li, B. Kurz, K. E. Kuettner, E. Frank, A. J. Grodzinsky, Vulnerability of the superficial zone of immature articular cartilage to compressive injury, *Arthritis Rheum.* 62 (2010) 3016–3027.
- [100] Y. Henrotin, B. Kurz, T. Aigner, Oxygen and reactive oxygen species in cartilage degradation: friends or foes?, *Osteoarthritis and Cartilage* 13 (8) (2005) 643–654.
- 945 [101] L. Zheng, Z. Zhang, P. Sheng, A. Mobasheri, The role of metabolism in chondrocyte dysfunction and the progression of osteoarthritis, *Ageing Res. Rev.* 66 (2021) 101249.
- [102] L. Liu, P. Luo, M. Yang, J. Wang, W. Hou, P. Xu, The role of oxidative stress in the development of knee osteoarthritis: A comprehensive research review, *Front. Mol. Biosci.* . 9 (2022) 1–11.
- 950 [103] J. P. Kosonen, A. S. Eskelinen, G. A. Orozco, M. C. Coleman, J. E. Goetz, D. D. Anderson, A. J. Grodzinsky, P. Tanska, R. K. Korhonen, Mechanobiochemical finite element model to analyze impact-loading-induced cell damage, subsequent proteoglycan loss, and anti-oxidative treatment effects in articular cartilage, *bioRxiv* (2024). doi:10.1101/2024.07.03.601852.
- 955 [104] M. H. Mohd Yunus, Y. Lee, A. Nordin, K. H. Chua, R. Bt Hj Idrus, Remodeling osteoarthritic articular cartilage under hypoxic conditions, *Int. J. Mol. Sci.* 23 (10) (2022).
- [105] K. Theodoridis, E. Aggelidou, M.-E. Manthou, A. Kritis, Hypoxia promotes cartilage regeneration in cell-seeded 3d-printed bioscaffolds cultured with a bespoke 3d culture device, *Int. J. Mol. Sci.* 24 (7) (2023).
- 960 [106] T. Fang, X. Zhou, M. Jin, J. Nie, X. Li, Molecular mechanisms of mechanical load-induced osteoarthritis, *Int. Orthop.* 45 (2021) 1125–1136.

- [107] B. Bartok, G. S. Firestein, Fibroblast-like synoviocytes: key effector cells in rheumatoid arthritis, *Immunol. Rev.* 233 (2010) 233–255.
- 965 [108] N. Parameswaran, S. Patial, Tumor necrosis factor- α signaling in macrophages, *Crit. Rev. Eukaryot. Gene Expr.* 20 (2010) 87–103.
- [109] H. Guo, J. Huang, Y. Liang, D. Wang, H. Zhang, Focusing on the hypoxia-inducible factor pathway: role, regulation, and therapy for osteoarthritis, *Eur. J. Med. Res.* 27 (2022) 288.
- 970 [110] X.-A. Zhang, H. Kong, Mechanism of hifs in osteoarthritis, *Front. Immunol.* 14 (2023).
- [111] J. Zhang, P. Gao, W.-R. Chang, J.-Y. Song, F.-Y. An, Y.-J. Wang, Z.-P. Xiao, H. Jin, X.-H. Zhang, C.-L. Yan, The role of hif-1 α in hypoxic metabolic reprogramming in osteoarthritis, *Pharmacol. Res.* 213 (2025) 107649.
- [112] B. Rodriguez-Vila, V. Gonzalez-Hospital, E. Puertas, J.-J. Beunza, D. M. Pierce, Democratization of deep learning for segmenting cartilage from mris of human knees: Application to data from the osteoarthritis initiative, *J. Orthop. Res.* 41 (8) (2023) 1754–1766.
- 975 [113] B. Rodriguez-Vila, P. Sánchez-González, I. Oropesa, E. J. Gomez, D. M. Pierce, Automated hexahedral meshing of knee cartilage structures – application to data from the osteoarthritis initiative, *Comput. Methods Biomech. Biomed. Engin.* 20 (14) (2017) 1543–1553.
- 980 [114] E. N. Blaney Davidson, van der Kraan P. M., van den Berg W. B., TGF- β and osteoarthritis, *Osteoarthritis and Cartilage* 15 (2007) 597–604.
- [115] H. A. Kim, Y. W. Song, Apoptotic chondrocyte death in rheumatoid arthritis, *Arthritis Rheum.* 42 (1999) 1528–1537.
- 985 [116] P. Malaviya, R. M. Nerem, Fluid-induced shear stress stimulates chondrocyte proliferation partially mediated via TGF-beta1, *Tissue Eng.* 8 (2002) 581–590.

- [117] M. Duan, Q. Wang, Y. Liu, J. Xie, The role of TGF- β 2 in cartilage development and diseases, *Bone Joint Res.* 10 (2021) 474–487.
- 990 [118] N. Verzijl, J. DeGroot, S. R. Thorpe, R. A. Bank, J. N. Shaw, T. J. Lyons, J. W. Bijlsma, F. P. Lafeber, J. W. Baynes, J. M. TeKoppele, Effect of collagen turnover on the accumulation of advanced glycation end products, *J. Biol. Chem.* 275 (2000) 39027–39031.
- [119] A. Maroudas, M. T. Bayliss, N. Uchitel-Kaushansky, R. Schneiderman, E. Gilav,
995 Aggrecan turnover in human articular cartilage: Use of aspartic acid racemization as a marker of molecular age, *Arch. Biochem. Biophys.* 350 (1998) 61–71.
- [120] C. B. Little, C. T. Meeker, S. B. Golub, K. E. Lawlor, P. J. Farmer, S. M. Smith, A. J. Fosang, Blocking aggrecanase cleavage in the aggrecan interglobular domain abrogates cartilage erosion and promotes cartilage repair, *J. Clin. Invest.* 117 (2007) 1627–1636.
- 1000 [121] A. R. Poynton, J. M. Lane, Safety profile for the clinical use of bone morphogenetic proteins in the spine, *Spine* 27 (2002) 40–48.
- [122] T. Shiba, D. Nishimura, Y. Kawazoe, Y. Onodera, K. Tsutsumi, R. Nakamura, M. Ohshiro, Modulation of mitogenic activity of fibroblast growth factors by inorganic polyphosphate, *J. Biol. Chem.* 278 (2003) 26788–26792.
- 1005 [123] L. M. Wakefield, T. S. Winokur, R. S. Hollands, K. Christopherson, A. D. Levinson, M. B. Sporn, Recombinant latent transforming growth factor beta 1 has a longer plasma half-life in rats than active transforming growth factor beta 1, and a different tissue distribution., *J. Clin. Invest.* 86 (1990) 1976–1984.
- [124] R. Fava, N. Olsen, J. Keski-Oja, H. Moses, T. Pincus, Active and latent forms of
1010 transforming growth factor beta activity in synovial effusions, *J. Exp. Med.* 169 (1989) 291–296.
- [125] R. Simó, A. Barbosa-Desongles, A. Lecube, C. Hernandez, D. M. Selva, Potential Role of Tumor Necrosis Factor- α in Downregulating Sex Hormone–Binding Globulin, *Diabetes* 61 (2012) 372–382.

- 1015 [126] R. Mehra, A. Storfer-Isser, H. L. Kirchner, N. Johnson, N. Jenny, R. P. Tracy, S. Redline, Soluble interleukin 6 receptor: A novel marker of moderate to severe sleep-related breathing disorder, *Arch. Intern. Med.* 166 (2006) 1725–1731.
- [127] D. J. Hazuda, J. C. Lee, P. R. Young, The kinetics of interleukin 1 secretion from activated monocytes. Differences between interleukin 1 α and interleukin 1 β , *J. Biol. Chem.* 263 (1988) 8473–8479.
- 1020 [128] N. Johansson, U. Saarialho-Kere, K. Airola, R. Herva, L. Nissinen, J. Westermarck, E. Vuorio, J. Heino, V.-M. Kähäri, Collagenase-3 (MMP-13) is expressed by hypertrophic chondrocytes, periosteal cells, and osteoblasts during human fetal bone development, *Dev. Dyn.* 208 (1997) 387–397.
- 1025 [129] C. Urbach, N. C. Gordon, I. Strickland, D. Lowne, C. Joberty-Candotti, R. May, A. Herath, D. Hijnen, J. L. Thijs, C. A. Bruijnzeel-Koomen, R. R. Minter, F. Hollfelder, L. Jermutus, Combinatorial Screening Identifies Novel Promiscuous Matrix Metalloproteinase Activities that Lead to Inhibition of the Therapeutic Target IL-13, *Chem. Bio.* 22 (2015) 1442–1452.
- 1030 [130] K. Yamamoto, K. Owen, A. E. Parker, S. D. Scilabra, J. Dudhia, D. K. Strickland, L. Troeberg, H. Nagase, Low density lipoprotein receptor-related protein 1 (lrp1)-mediated endocytic clearance of a disintegrin and metalloproteinase with thrombospondin motifs-4 (adamts-4): Functional differences of non-catalytic domains of adamts-4 and adamts-5 in lrp1 binding*, *J. Bio. Chem.* 289 (2014) 6462–6474.
- 1035 [131] C. M. Doherty, R. Visse, D. Dinakarandian, D. K. Strickland, H. Nagase, L. Troeberg, Engineered Tissue Inhibitor of Metalloproteinases-3 Variants Resistant to Endocytosis Have Prolonged Chondroprotective Activity, *J. Bio. Chem.* 291 (2016) 22160–22172.